Surrogate Modeling for Large-Scale Black-Box Systems

by

Rhea Patricia Liem

Submitted to the School of Engineering
in Partial Fulfillment of the Requirements for the degree of

Master of Science in Computation for Design and Optimization

at the

MASSACHUSETTS INSTITUTE OF TECHNOLOGY

September 2007

Author .....
School of Engineering
August 10, 2007

Certified by .....
Karen E. Willcox
Associate Professor
Thesis Supervisor

Accepted by .....
Jaime Peraire
Professor of Aeronautics and Astronautics
Co-Director, Computation for Design and Optimization

Surrogate Modeling for Large-Scale Black-Box Systems

by

Rhea Patricia Liem

Submitted to the School of Engineering
on August 10, 2007, in partial fulfillment of the
requirements for the degree of
Master of Science in Computation for Design and Optimization

Abstract

This research introduces a systematic method to reduce the complexity of large-scale black-box systems for which the governing equations are unavailable. For such systems, surrogate models are critical for many applications, such as Monte Carlo simulations; however, existing surrogate modeling methods often are not applicable, particularly when the dimension of the input space is very high. In this research, we develop a systematic approach to represent the high-dimensional input space of a large-scale system by a smaller set of inputs. This collection of representatives is called a *multi-agent collective*, forming a surrogate model with which an inexpensive computation replaces the original complex task. The mathematical criteria used to derive the collective aim to avoid overlapping of characteristics between representatives, in order to achieve an effective surrogate model and avoid redundancies.

The surrogate modeling method is demonstrated on a flight inventory that contains flight data corresponding to 82 aircraft types. Ten aircraft types are selected by the method to represent the full flight inventory for the computation of fuel burn estimates, yielding an error between outputs from the surrogate and full models of just 2.08%. The ten representative aircraft types are selected by first aggregating similar aircraft types together into *agents*, and then selecting a representative aircraft type for each agent. In assessing the similarity between aircraft types, the characteristic of each aircraft type is determined from available flight data instead of solving the fuel burn computation model, which makes the assessment procedure inexpensive. Aggregation criteria are specified to quantify the similarity between aircraft types and a stringency, which controls the tradeoff between the two competing objectives in the modeling—the number of representatives and the estimation error.

The surrogate modeling results are compared to a model obtained via manual aggregation; that is, the aggregation of aircraft types is done based on engineering judgment. The surrogate model derived using the systematic approach yields fewer representatives in the collective, yielding a surrogate model with lower computational cost, while achieving better accuracy. Further, the systematic approach eliminates the subjectivity that is inherent in the manual aggregation method. The surrogate model is also applied to other flight inventories, yielding errors of similar magnitude to the case when the reference flight inventory is considered.

Thesis Supervisor: Karen E. Willcox
Title: Associate Professor

Acknowledgments

My gratitude goes to all people who have provided me with support, technical or otherwise, for the completion of this thesis. I owe a great deal of thanks especially to my thesis advisor, Prof. Karen Willcox, for her advises—both technical and in scientific writing, insightful comments, and encouragement. I would also like to thank Douglas L. Allaire, for the many discussions and answers, especially about APMT and SAGE. I have also received helpful support from Sathya Balasubramanian and his colleagues from The Volpe National Transportation Systems Center, to whom I extend my gratitude. It was a pleasure for me to work with the APMT team at MIT; the Wednesday meetings have given me many insights into aviation environmental impact and statistical analyses.

This research has been possible with funding from the Singapore-MIT Alliance (SMA). I would like to thank Ms. Jocelyn Sales, Manager of SMA Graduate Students and Events at MIT; and Mr. Michael Lim, SMA Management Support Officer in Singapore for their constant administrative support.

I am also very grateful with the help from Ms. Laura Koller, CDO Administrator; and Ms. Jean Sofronas, Administrative Assistant for ACDL lab, who have provided administrative support for students, and whose hard work is often left unmentioned.

Lastly, for my entire family, and my friends (in Jakarta, Singapore, Boston, and others), thank you for being there, for your overflowing love, support, and faith in me. To my international mix of friends at MIT, thank you for sharing our differences and making my life here more colorful.

This work was supported in part by the Office of Environment and Energy, U.S. Federal Aviation Administration under Contract No. DTFAWA-05-D-00012, Task Order 0002 managed by Maryalice Locke. Any opinions, findings, and conclusions or recommendations expressed in this material are those of the author and do not necessarily reflect the views of the FAA.

Contents

List of Figures

List of Tables

Nomenclature

A	a set of units (aircraft types/AE pairs) that belong to an agent
CO	Carbon Monoxide
CO_2	Carbon Dioxide
C_D	drag coefficient
C_L	lift coefficient
C_{D0}	parasitic drag coefficient
C_{D2}	induced drag coefficient
C_{f1}	first fuel flow coefficient in BADA
C_{f2}	second fuel flow coefficient in BADA
C_{f3}	first descent fuel flow coefficient in BADA
C_{f4}	second descent fuel flow coefficient in BADA
Co	a set containing common members between minor and major agents
D	drag force
E	emissions
$EICO$	Emissions Index for CO
$EIHC$	Emissions Index for HC
$EINO_x$	Emissions Index for NO_x
F	thrust
H	humidity factor
HC	Hydrocarbons
H_2O	water
Ma	major agent
$Mach$	Mach number
Mi	minor agent

NO_x	Nitrogen Oxides
N_f	number of flights within a unit (aircraft type/AE pair)
N_{AC}	number of aircraft types in a data set
N_{AE}	number of AE pairs in a data set
N_{agent}	number of agents formed by the surrogate modeling method
$REICO$	Referred Emissions Index for CO
$REIHC$	Referred Emissions Index for HC
$REINO_x$	Referred Emissions Index for NO_x
R^2	coefficient of determination
S	aircraft wing area
SFC	Specific Fuel Consumption
SO_x	Sulfur Oxides
V	flight speed
W_{ff}	corrected fuel flow rate
ΔV	change in flight speed
Δ_h	change in altitude
Δ_t	elapsed time
Ξ_{2000}	flight information data set from SAGE Flight Inventory from 2000
Ξ_{2001}	flight information data set from SAGE Flight Inventory from 2001
Ξ_{2002}	flight information data set from SAGE Flight Inventory from 2002
Ξ_{2003}	flight information data set from SAGE Flight Inventory from 2003
Ξ_{2004}	flight information data set from SAGE Flight Inventory from 2004
Ξ_{2005}	flight information data set from SAGE Flight Inventory from 2005
Ξ_{CFDR}	flight information data set from the Computer Flight Data Recorder
β_0	constant term of the linear regression equation
β_1	gradient of the linear regression equation
δ	pressure ratio (ambient to sea-level)
δ_t	threshold value
γ	gradient ratio
$\mathbf{E}$	total emissions
$\mathbf{f}$	total fuel burn

ρ	air density
σ	standard deviation
θ	temperature ratio (ambient to sea-level)
$\tilde{f}$	estimated fuel burn
$\tilde{E}$	estimated emissions
$\tilde{\mathbf{E}}$	estimated total emissions
$\tilde{\mathbf{f}}$	estimated total fuel burn
ε	total estimation error
ε_c	cross-estimation error
b_0	selected constant term of the linear regression equation
b_1	selected gradient of the linear regression equation
f	fuel burn
g	gravitational acceleration constant
h	flight altitude
m	aircraft mass
AE	aircraft/engine
AEDT	Aviation Environmental Design Tool
AFE	Above Field Elevation
APMT	Aviation Environmental Portfolio Management Tool
BADA	Base of Aircraft Data
BFFM2	Boeing Fuel Flow Method 2
BVB	Benefits Valuation Block
CFDR	Computer Flight Data Recorder
DOE	Design of Experiments
EDS	Environmental Design Space
EI	Emissions Index
ETMS	Enhanced Traffic Management System
FAA-AEE	Federal Aviation Administration Office of Environment and Energy
GC	Great Circle
ICAO	International Civil Aviation Organization
ISA	International Standard Atmosphere

MSL	Mean Sea Level
MTOW	Maximum Take-off Weight
OAG	Official Airline Guide
PEB	Partial Equilibrium Block
REI	Referred Emissions Index
SAE AIR	Society of Automative Engineers Aerospace Information Report
SAGE	System for assessing Aviation's Global Emissions
TOGW	Take-off Gross Weight

Chapter 1

Introduction

1.1 Motivation

The advancement of numerical simulation has assisted considerably the study of many complex physical phenomena and is becoming increasingly widespread as a means to support decision-making and policy-making processes. Such computational models are often complex, involving many disciplines, many input parameters, and long computation times. For example, the Aviation Environmental Portfolio Management Tool (APMT) is a computational model being developed to support aviation environmental policy-making by providing the capability to evaluate the impacts of environmental policy alternatives in the form of social costs, such as public and private mitigation costs and public environmental benefits [53]. The scale and complexity of the required analyses are immense; for example, simulation of one year involves over 35 million flights with approximately 350 aircraft types and thousands of input parameters, analyzed with black-box models spanning airline economics, environmental economics, aircraft operations, aircraft performance and emissions, noise, local air quality, and global climate. Furthermore, characterization of uncertainty is an important element of a decision-support tool such as APMT, making the computational burden even greater.

Surrogate models of lower complexity that are inexpensive to evaluate and approximate accurately the large-scale model can greatly facilitate analysis tasks at hand. Such analyses include Monte Carlo simulations that require many thousands of scenarios to characterize the effects of input uncertainty. These simulations, when using the large-scale model, are intractable. Surrogate modeling methodologies have been shown to be effective approaches

for computationally expensive models, such as jet propulsion [50] and airfoil design [42]. Despite these demonstrated successes, a key remaining challenge is the derivation of surrogate models for large-scale black-box systems with very high-dimensional input parameter space. This challenge must be addressed before surrogate modeling can be applied to large-scale computational systems such as APMT.

1.2 Surrogate Modeling

As proposed in [13], surrogate models can be divided into three categories. First, data-fit models are typically computed using interpolation or regression of data generated by solving the large-scale system at a set of sample points [51]. The sample points are often generated using a design of experiments. Second, reduced-order models can be derived using systematic methods to approximate the input/output relationship while reducing the order of the original system. An overview of model reduction methods is provided in [1]. The third category of surrogate models comprises hierarchical models, which are also called multifidelity, variable-fidelity, or variable-complexity models [45, 46]. A brief overview of the three categories of surrogate modeling methodologies is given in the following subsections.

1.2.1 Data-Fit Surrogate Models

Figure 1-1 illustrates the general concept behind the construction of a data-fit surrogate model. Four key steps in constructing such a model are enumerated in [44]: Design of Experiments (DOE), numerical simulations, construction of the surrogate model, and model validation. DOE is used to select a set of sample points, at which the large-scale analysis is performed. A review of various sampling methods for DOE is summarized in [47]. The surrogate models can then be constructed from the sampled data points using parametric techniques, such as polynomial regression and Kriging [11, 33]; and non-parametric techniques, such as projection-pursuit regression [21] and radial basis functions [40]. See, for example, [44] for an overview of many of these methods. While data-fit surrogates can be derived for black-box models, a significant challenge remains in sampling from a high-dimensional parametric input space. When the number of input parameters increases beyond a handful, DOE techniques must be applied with care in order to balance the computational cost of the required simulations with coverage of the input space. For a system

such as APMT, which has many thousands of inputs, building a surrogate model using sampling is not a viable approach due to the computational complexity.

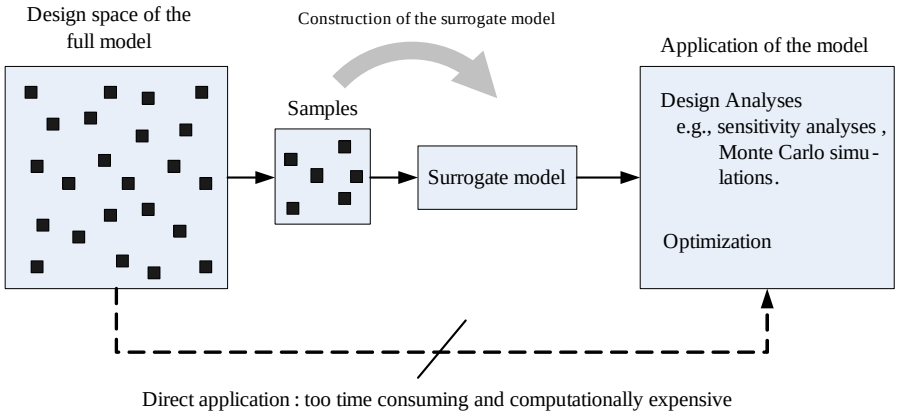

Figure 1-1: Construction of a data-fit surrogate model.

1.2.2 Model Reduction

Model reduction can be applied to dynamical systems to determine surrogate models that preserve the relationships between system inputs and outputs, as illustrated in Figure 1-2. Most reduction methods for large-scale systems derive the reduced model by projecting the large-scale model onto a basis that spans a space of lower dimension. The reduced space basis can be computed using a number of different methods, including Krylov-subspace methods [18, 22, 24], approximate balanced truncation [25, 36, 43, 49], and proper orthogonal decomposition [12, 26, 48].

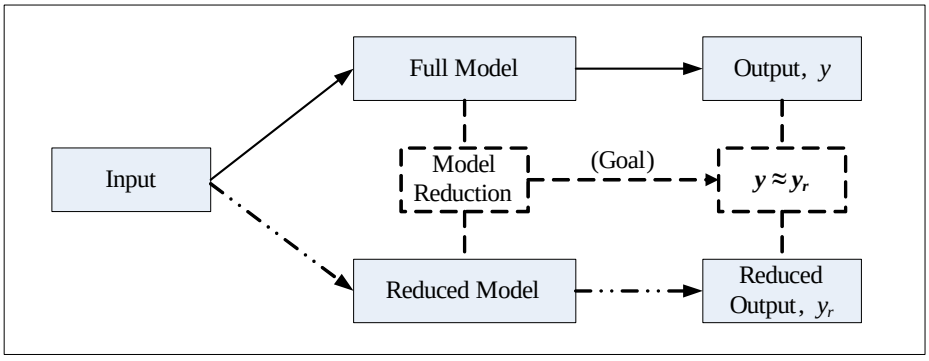

Figure 1-2: Model reduction applied to dynamical systems.

While model reduction methods have been developed for nonlinear problems [6], rigorous

methods that extend beyond the well studied linear time-invariant case remain largely an open challenge. Black-box models, where knowledge of the system's governing equations is absent, and systems with many input parameters present a further challenge for existing model reduction methods.

1.2.3 Hierarchical Models

There are several methods to construct the hierarchical models, depending on the specific computational task at hand. The same high-fidelity model but with a higher residual tolerance for the convergence can be used as the low-fidelity model [20]. The low-fidelity model can also be derived using a simplified mathematical model, e.g., a coarser grid in a finite element model [3, 4, 9, 35], or a simpler engineering model that neglects some physics modeled by the high-fidelity method [5]. See, for example, [10] for a demonstration of variable-fidelity models on a supersonic business jet problem.

1.3 Thesis Objectives

This research aims to devise a systematic method to create surrogate models for large-scale black-box systems that have a very large number of input parameters. For such systems, existing model reduction methods cannot be applied due to their dependence on the structure of the governing equation of the system. Data-fit techniques break down due to an inability to sample adequately the input parameter space.

As illustrated in Figure 1-3, our approach focuses on a systematic methodology to reduce the dimension of the input space. For some problems, reduction of the input space yields directly a hierarchical surrogate model of lower computational complexity; for other cases, our approach leads to an intermediate system of lower input dimension to which a data-fit surrogate modeling method could subsequently be applied.

The specific objectives of this thesis are to:

1. Create surrogate models for large-scale black-box systems that have a very large number of input parameters. In particular, this thesis proposes a systematic method to reduce the dimension of the input space.

2. Demonstrate the proposed methodology by applying it to create surrogates of the aircraft fuel burn and emissions models within APMT.

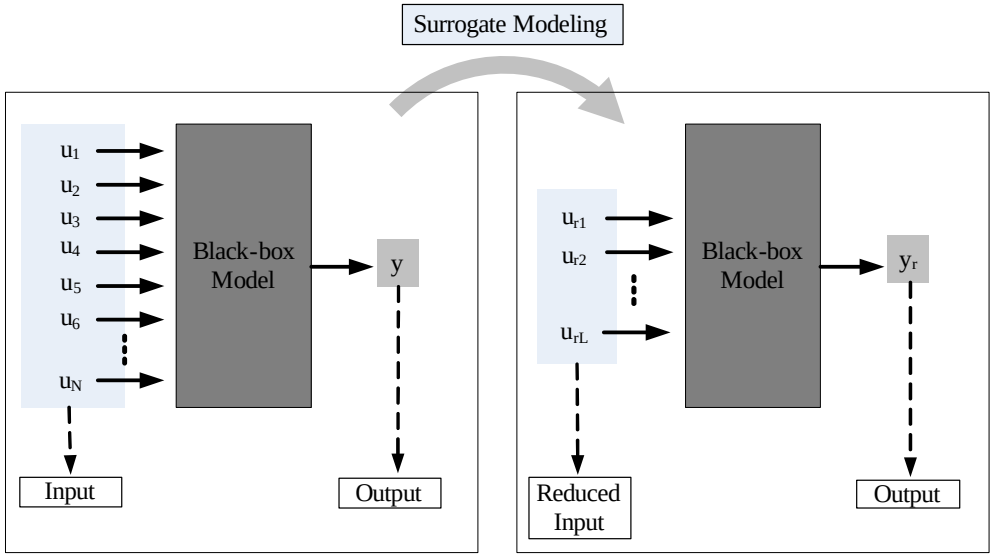

Figure 1-3: Surrogate modeling of a large-scale black-box system via reduction of the input space.

1.4 Outline of the Thesis

Chapter 2 describes the available tools to study aviation environmental impact. An overview of the architecture of APMT, which is the system of interest in our case studies, is presented. The model used within APMT for fuel burn and emissions computations is described, along with the training data sets used in the development of this research.

The surrogate modeling method developed in this research is presented in Chapter 3. Specifically, the chapter discusses the formation of a *multi-agent collective*, where the idea of aggregation is used to reduce the computational complexity of large-scale problems. A brief overview of collectives is provided before the chapter elaborates on the details of the developed procedure.

Chapter 4 describes the application of the surrogate modeling method to the fuel burn estimation model within APMT. The chapter describes the implementation of the developed procedure, tailored to this first case study. The surrogate model derived based on the selected data set, with the corresponding estimation error that rates the performance of the model, are then presented. Here, the assessments of the surrogate model are also provided. The second case study, a surrogate modeling for emissions estimation, is discussed next in Chapter 5.

Finally, in Chapter 6 conclusions and recommendations for future work are presented.

Chapter 2

Aviation System Model for Environmental Impact

In this chapter, the available tools to study aviation environmental impact are briefly described. This chapter first provides an overview of the Aviation Environmental Portfolio Management Tool (APMT) architecture. It then describes the System for assessing Aviation's Global Emissions (SAGE), the modeling tool used for computing aircraft fuel burn and emissions within APMT. Finally, the data sets that are used in the development of this research are described.

2.1 Overview of APMT Architecture

The Federal Aviation Administration Office of Environment and Energy (FAA-AEE) is developing a suite of tools to evaluate the impacts of policy decisions on aviation and the environment [52]. The central building block of these tools comprises three main functional components: the Environmental Design Space (EDS), the Aviation Environmental Design Tool (AEDT), and APMT. A simplified schematic of the tools suite is provided in Figure 2-1. EDS is an aircraft and engine analysis tool that provides estimates of aircraft performance tradeoffs for different technology assumptions and policy scenarios. In AEDT, aviation noise and emissions are estimated based on detailed fleet descriptions and flight schedules. These estimated inventories are made at both global and local levels. APMT serves as a framework to provide support to the international policy decision-making processes through assessments of interdependencies among aviation-related environmental impacts

under different policy, technology, operations, and market scenarios [30]. The environmental impacts encompassed in the analyses are local air quality, community noise, and climate change. Two main blocks within APMT are the Partial Equilibrium Block (PEB), which simulates economic flows in the aviation markets; and the Benefits Valuation Block (BVB), which performs benefit-cost assessments and monetizes health and welfare impacts based on emissions and noise quantities. The information flows between the tools are illustrated in Figure 2-1. SAGE, which assesses aviation fuel burn and emissions, is a tool within AEDT that is considered in this research. A brief overview of SAGE is provided in the following section.

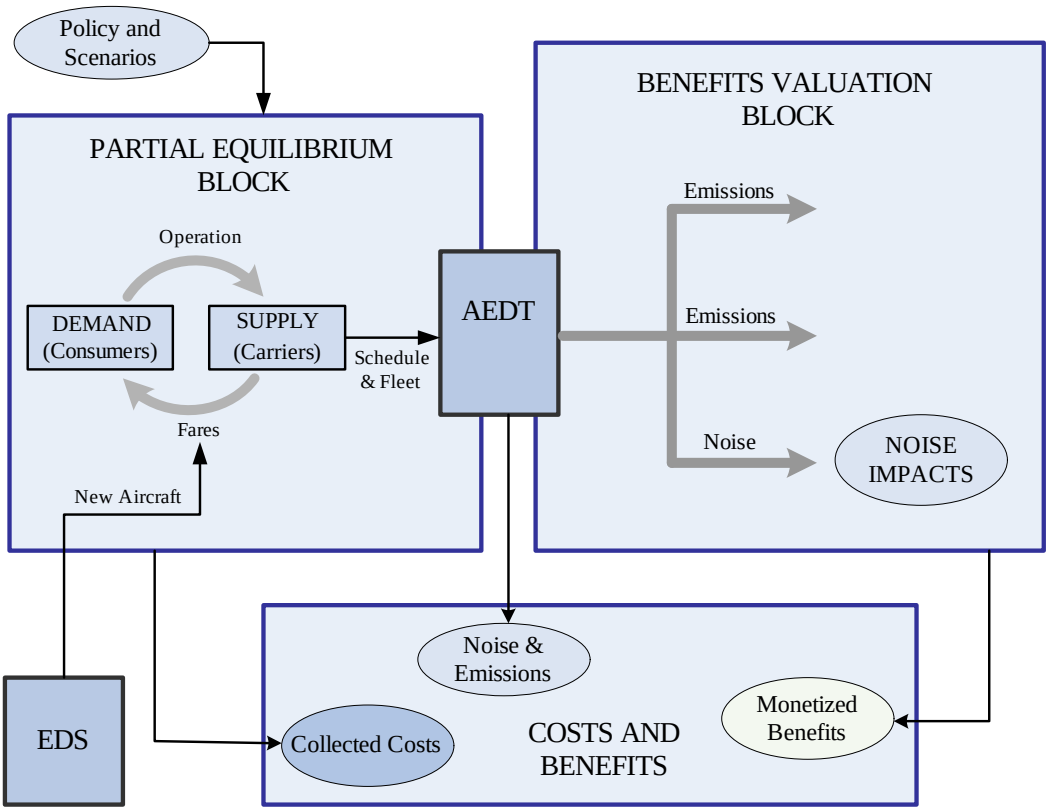

Figure 2-1: Schematic of the components of the FAA Environmental Tool Suite [30].

2.2 Overview of SAGE

SAGE is an internationally accepted model used for estimating aircraft fuel burn and emissions [17]. The quantities computed by SAGE are fuel burn and emissions for Carbon

Monoxide (CO), Carbon Dioxide (CO_2), Nitrogen Oxides (NO_x), Hydrocarbons (HC), water (H_2O), and Sulfur Oxides (SO_x). The flight trajectory in SAGE is defined by its gate-to-gate flight profile, where the flight movement is divided into five main segments: terminal departure, en-route climb, cruise, en-route descent, and terminal arrival. This profile is shown in Figure 2-2. All segments, excluding cruise, are further divided into two subsegments. The numbered points in Figure 2-2 are altitude-dependent segmentation points. Table 2.2 provides the altitude details corresponding to each point. MSL and AFE, mentioned in Table 2.2, refer to Mean Sea Level and Above Field Elevation, respectively.

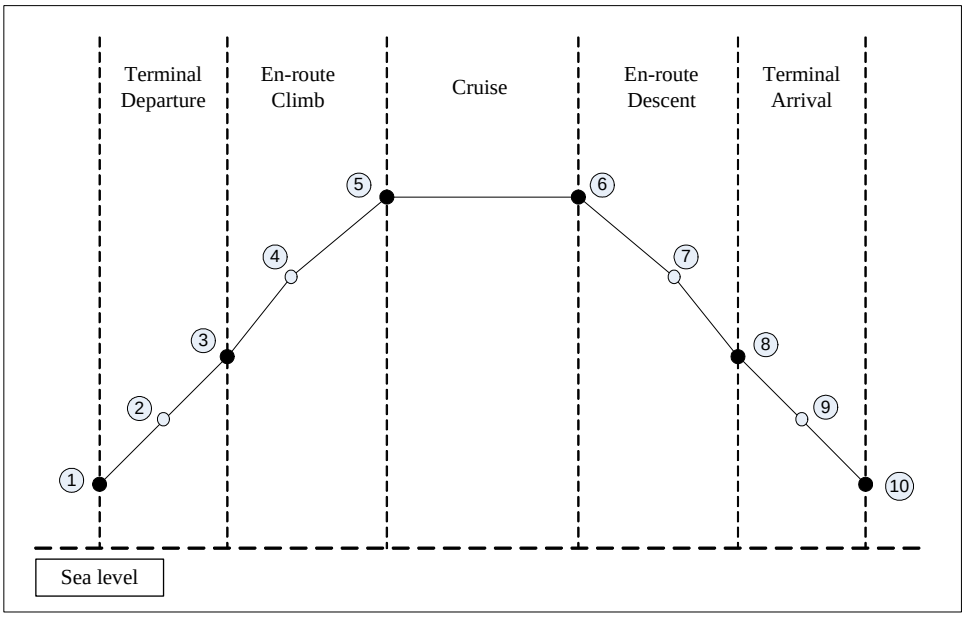

Figure 2-2: Diagram for a gate-to-gate flight profile.

No	Description
1	0 ft AFE
2	Airport's mixing height
3	10,000 ft AFE
4	Mach transition altitude
5	User-defined cruise altitude (in MSL)
6	User-defined cruise altitude (in MSL)
7	Mach transition altitude
8	10,000 ft AFE
9	Airport's mixing height
10	0 ft AFE

Table 2.1: The altitude descriptions for the points specified in Figure 2-2.

The trajectory information that is required for computations performed in SAGE is obtained from the Enhanced Traffic Management System (ETMS). ETMS contains radar-based data on flight positions, which are a combination of flight-identifier encoded radar position reports and a flight's filed flight plan. ETMS captures every aircraft that flies within the coverage of FAA radar, including unscheduled, cargo, military, charter and scheduled flights [17]. Flights that do not enter radar-controlled airspace, but file a flight plan, are also included in ETMS data. The dispersed Great Circle (GC) trajectory is used whenever ETMS data are absent. The GC trajectory is essentially the shortest line fit through two points on the earth's surface. A dispersion method that uses a randomly assigned route other than the GC is introduced in SAGE to make the GC trajectory modeling more realistic. The dispersion is done using pseudo-random numbers that generate a deviation from the actual GC route [17].

The computational data flow for fuel burn and emissions calculations in SAGE is briefly summarized in Figure 2-3. The primary data sources for the computations are the International Civil Aviation Organization (ICAO) emissions and fuel flow databank; and Eurocontrol's Base of Aircraft Data (BADA) [17]. The ICAO databank contains both fuel flow and emissions information, including the Emissions Indices (EI) for various engine types. ICAO developed its databank from data collected from various engine manufacturers. BADA contains the coefficients for performance and operating procedures associated with 186 different aircraft types [15]. BADA specifies coefficients for calculating thrust, drag, fuel flow, and nominal speeds during climb, cruise, and descent [29].

Ambient temperature, pressure, density, and speed of sound are required in computing fuel burn and emissions in SAGE. These atmospheric quantities are computed by an atmospheric module, in which the International Standard Atmosphere (ISA) with no wind is assumed [17]. Another assumption that is required is the Take-off Gross Weight (TOGW). The stage-based TOGW information is obtained from the Society of Automative Engineers Aerospace Information Report (SAE AIR) 1845 [34]. The total fuel burn (f), in kg, for each flight is estimated as

$$f = SFC \cdot F \cdot \Delta t, \tag{2.1}$$

where the inputs are Specific Fuel Consumption (SFC), thrust (F), and the elapsed time

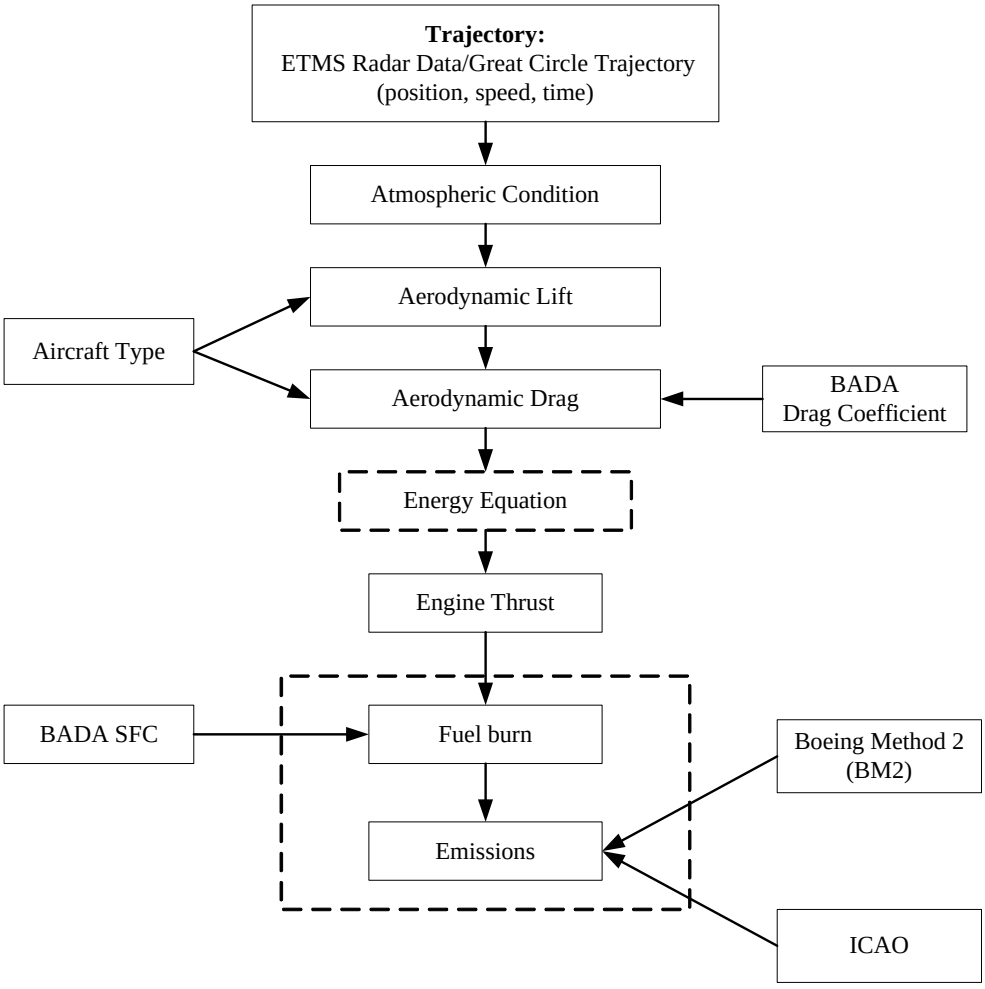

Figure 2-3: SAGE computational data flow for fuel burn and emissions calculation.

(Δt). In BADA, SFC is specified by a first-order polynomial model that is a function of flight Mach number and altitude [15]:

$$SFC = C_{f_1} \cdot \left(1 + \frac{V}{C_{f_2}}\right). \tag{2.2}$$

Factors that affect SFC values are engine throttle setting and flight speed (V). The SFC coefficients, C_{f1} and C_{f2}, shown in Equation 2.2 are obtained from BADA. During cruise, a thrust reduction factor is applied to the equation. A different equation is used if the calculated thrust falls below 7% of maximum thrust during descent. For the minimum fuel flow (low power engine) setting, the SFC is computed as:

$$SFC = C_{f3} \cdot \left(1 - \frac{h}{C_{f4}}\right) \quad \text{(for minimum fuel flow)}, \tag{2.3}$$

where C_{f3} and C_{f4} are BADA SFC coefficients, and h refers to the flight altitude. Equation 2.3 shows that the minimum fuel flow is only a function of altitude. Thus, this equation is not very accurate for idle and taxi modes.

To calculate thrust at a particular flight position, SAGE uses an energy equation as expressed in the following equation,

$$(F - D) \cdot V = m \cdot g \cdot \frac{\Delta h}{\Delta t} + m \cdot V \cdot \frac{\Delta V}{\Delta t}, \tag{2.4}$$

where Δh is the change in altitude, ΔV is the change in flight speed, m is the aircraft mass, and g is the gravitational acceleration constant. Equation 2.4 obtains thrust by enforcing an equilibrium between thrust and drag while considering the changes in kinetic and potential energy. Before applying this equation, the following computation for the drag force, D, is required,

$$D = C_D \frac{\rho V^2 S}{2}, \tag{2.5}$$

which takes the air density (ρ), the wing area (S), and the drag coefficient (C_D) as inputs. The equation to obtain this value is

$$C_D = C_{D0} + C_{D2} \cdot (C_L)^2, \tag{2.6}$$

where the coefficients C_{D0} and C_{D2} are obtained from BADA. The drag coefficient is computed separately for each take-off, climb-out, cruise, approach, and landing configurations, as BADA assigns different C_{D0} and C_{D2} values for different flight segments. The lift coefficient (C_L) is computed as:

$$C_L = \frac{2mg}{\rho V^2 S}. \tag{2.7}$$

The calculated thrust and the BADA SFC are then used to compute fuel burn. The computed fuel burn reflects both technology levels (propulsion, aerodynamics, controls, and structures) and operational practices (speed and altitude) of the airplane. This conclusion is derived from the fact that the thrust required is determined by aerodynamic drag, operation weight, and aircraft dynamics [17].

Having obtained the estimation of total fuel burn, the emissions values can then be calculated. The primary products of the combustion process include CO_2 and H_2O. The emissions calculation for these two species is similar to the equation to estimate the emissions of the SO_x. This latter family of species typically results from aviation fuel sulfur impurities. CO_2, H_2O, and SO_x emissions values are essentially determined from mass balance of the chemical species in the fuel and the exhaust [34]. The emissions values, in g, for these species are obtained by multiplying the fuel burn values by constant emissions indices, which are tabulated in Table 2.2.

Species	EI
CO_2	3155 g/kg of fuel
H_2O	1237 g/kg of fuel
SO_x	0.8 g/kg of fuel

Table 2.2: Emissions Indices for CO_2, H_2O, and SO_x.

The calculations for CO, NO_x, and HC emissions require information about the corresponding engine conditions at the specified atmospheric and flight conditions and the fuel burn rate (fuel flow) [17]. For these calculations, SAGE employs the Boeing Fuel Flow Method 2 (BFFM2), or the "Boeing curve fitting method". Engine performance and emissions data obtained via full-scale engine tests at ground level are the bases for BFFM2 [34]. The ICAO Emissions databank provides information about fuel flow data taken at the four certified power settings at sea-level static conditions. This method is able to calculate the

emissions of the full range of power settings while correcting for atmospheric conditions [32]. In SAGE, a correction is introduced to the BADA fuel flow ($SFC \cdot F$) to account for ambient temperature, pressure, and flight Mach number. The corrected fuel flow rate (W_{ff}) is obtained by:

$$W_{ff} = \frac{SFC \cdot F}{\delta} \cdot \theta^{3.8} \cdot e^{0.2 \cdot (Mach)^2}, \tag{2.8}$$

where θ is the temperature ratio (ambient to sea-level), δ is the pressure ratio (ambient to sea-level), and $Mach$ is the Mach number. The emissions indices ($EINO_x$, $EIHC$, and $EICO$) are obtained by first correlating the corrected fuel flow with referred emissions indices ($REINO_x$, $REIHC$, and $REICO$) obtained by applying BFFM2. BFFM2 uses an interpolation on the emissions indices versus fuel flow curve to obtain a referred emissions index (REI) value at a specific corrected fuel flow value [32]. The emissions indices that are used in the actual emissions computation are obtained by correcting the REI values to take the atmospheric conditions into account. To achieve this, Equations 2.9 to 2.11 are used for each species. H refers to the humidity factor, and other variables are as previously defined.

$$EINO_x = REINO_x \cdot e^H \cdot \left(\frac{\delta^{1.02}}{\theta^{3.3}} \right)^{0.5} \tag{2.9}$$

$$EIHC = REIHC \cdot \frac{\theta^{3.3}}{\delta^{1.02}} \tag{2.10}$$

$$EICO = REICO \cdot \frac{\theta^{3.3}}{\delta^{1.02}} \tag{2.11}$$

Total emissions are computed by multipying the corrected emissions indices by the computed fuel burn values as shown in Equations 2.12 to 2.14.

$$NO_x = EINO_x \cdot f \tag{2.12}$$

$$HC = EIHC \cdot f \tag{2.13}$$

$$CO = EICO \cdot f \tag{2.14}$$

To obtain global fuel burn and emissions inventories annually, the tools need to simulate the flights of all aircraft flown worldwide. The required computations can be massive for several reasons. First, there are millions of flights to be flown in the simulation. A year's flight inventory typically has approximately 350 distinct aircraft types. Considering the engine types associated with each aircraft type, we may have three times as many distinct aircraft/engine (AE) pairs. Second, the tools also need to read from and write to large databases. These processes add to the necessary computation time considerably. While it is feasible to run simulations of a handful of scenarios and use these models in an analysis mode, in many situations the computational cost of the required computations becomes prohibitive. For example, to characterize the effects of uncertainty, one might wish to perform a Monte Carlo simulation, requiring many thousands of simulations to be run.

To compute the emissions estimates for the yearly global aircraft fleet, the model requires approximately five hours to simulate one year of flights on a desktop computer. Thus, 1,000 runs in a Monte Carlo simulation, for example, would require approximately 7 months to complete; and the required runtime for 10,000 runs would be close to six years. Even with parallel implementation, these runtimes are still highly impractical. If the number of flights to be analyzed within each simulation can be reduced substantially, we could then reduce the runtimes of the aircraft performance models. Since characterizing the effects of uncertainty is a critical part of a decision support tool such as APMT, it is, therefore, imperative to create surrogate models that can reduce the number of required simulations while still maintaining accurate estimations of the inventories.

2.3 Training Data Sets

The development of the surrogate modeling method requires large data sets of flight information. The scope of this research is limited to the cruise segment of the flight (refer to Figure 2-2). Two types of data sets are used in the development of this research:

1. The Computer Flight Data Recorder (CFDR) data (Ξ_{CFDR})

   This data set contains one year of flight information data from an airline carrier's record, where information for each flight is constructed from the corresponding chord-by-chord data corresponding to that particular flight. A chord is defined as a segment of an aircraft's flight profile or trajectory containing geometric (e.g., latitude, longi-

tude, altitude) and performance (e.g., speed) information [17]. The flight information used in this research are cruise distance, cruise segment fuel flow and elapsed time. This data set records the actual fuel burn rate computed during flights.

2. SAGE Flight Inventory

   In SAGE Flight Inventories, all flight data are aggregated on a monthly basis. As opposed to the fuel flow information provided by the CFDR data, the fuel burn values that are provided in these data sets are obtained by following the SAGE fuel burn computation method as described in the previous section. For this research, only aircraft types with a capacity of more than 100 passengers are included, yielding at most 82 aircraft types per year. We use SAGE Flight Inventories from the years 2000 through 2005, denoted as Ξ_{2000} through Ξ_{2005}.

Table 2.3 summarizes the total number of aircraft types and flights used in this research. Ξ_{CFDR}, which is the smallest data set, is primarily used prior to the implementation of the method on a larger data set, i.e., Ξ_{2005}. The Ξ_{2000}, Ξ_{2001}, Ξ_{2002}, Ξ_{2003}, and Ξ_{2004} data sets are used for assessing the developed method, which is done by applying the surrogate model derived based on Ξ_{2005} to these flight inventories. The errors obtained from these implementations help to demonstrate the effectiveness of the surrogate modeling methodology, which will be described in the following chapter.

	Number of Aircraft Types	Number of Flights
Ξ_{CFDR}	11	2,329
Ξ_{2000}	78	15,336,117
Ξ_{2001}	79	15,216,780
Ξ_{2002}	80	15,309,512
Ξ_{2003}	82	15,866,325
Ξ_{2004}	82	16,397,737
Ξ_{2005}	82	17,719,921

Table 2.3: Number of aircraft types and flights for each data set used in this research.

Chapter 3

Multi-Agent Collectives: Surrogate Modeling by Aggregation

The idea of aggregation is used in this research as an approach to reduce the computational complexity of large-scale systems. Specifically, the aim is to create a *multi-agent collective* from the system of interest to form a surrogate model. This chapter begins by providing a brief overview of collectives. The method to create the surrogate model is then described in detail.

3.1 Multi-Agent Collective

A *collective* is broadly defined in [8] as "a multi-agent system where each agent is self-interested and capable of learning". In the context of Artificial Intelligence, Ferber [19] describes an *agent* as a physical or virtual entity that is only a partial representation of the environment, and is capable of acting in the environment. In this research, a multi-agent collective is created from a system that is constructed by a number of units, where a unit is defined as the smallest entity within a system that is unique and distinguishable from other units. The agents are then formed by aggregating similar units together, as illustrated in Figure 3-1. The formed agents, collectively, are required to replicate the computation performed by the full system. In this thesis, this computation will subsequently be referred to as the *collective computational task*.

As an example of a collective computational task, consider the computation of fuel burn estimates for the global aircraft fleet over a year of operations. This computational task is

performed by a simulation system comprising a number of aircraft types. In this system, the aircraft types are considered as the units, which can be aggregated to form agents. The collective computational task of estimating the total fuel burn is then carried out by using each agent, i.e., a group of similar aircraft types, to estimate the fuel burn for that group of aircraft types. This distribution of the collective computational task amongst a small number of agents enables a reduction in computational cost, as compared to the computation performed by the full system.

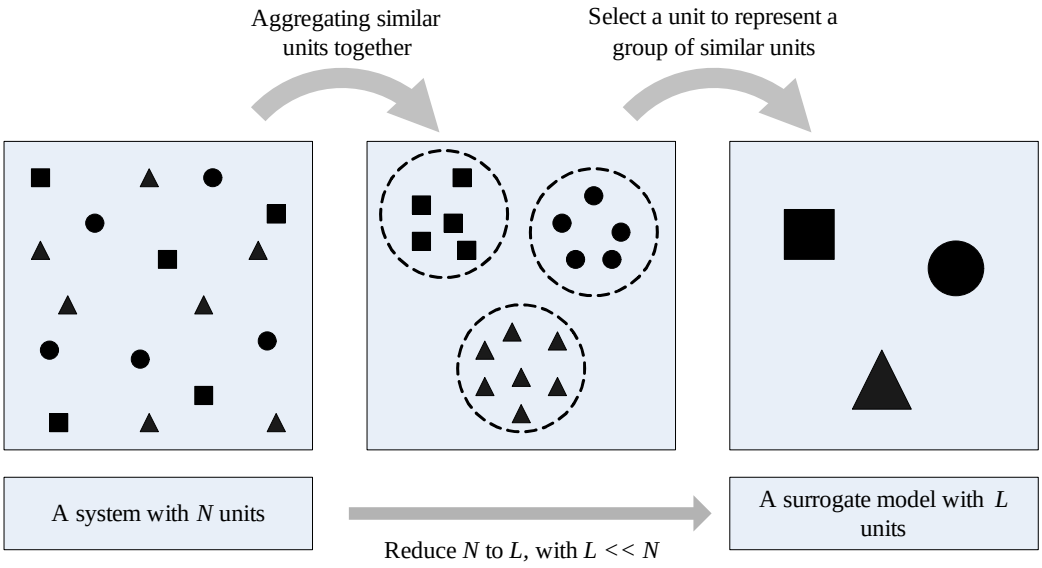

Figure 3-1: Reducing the dimension of input of a system by aggregating similar units together, and selecting representative units.

3.2 Surrogate Modeling Method

Figure 3-2 provides a general overview of the surrogate modeling method developed in this research. In essence, there are three steps in creating the surrogate model: the selection of an entity within a system to be the aggregation unit, the aggregation procedure to form agents, and the distribution of the collective computational task amongst agents. Engineering judgment plays an important role in selecting the appropriate unit, as the knowledge about the system and the collective computational task is a major consideration. The output from the procedure is a multi-agent collective, with which the collective computational task will be performed. More detailed procedures for each step are provided in the following

subsections.

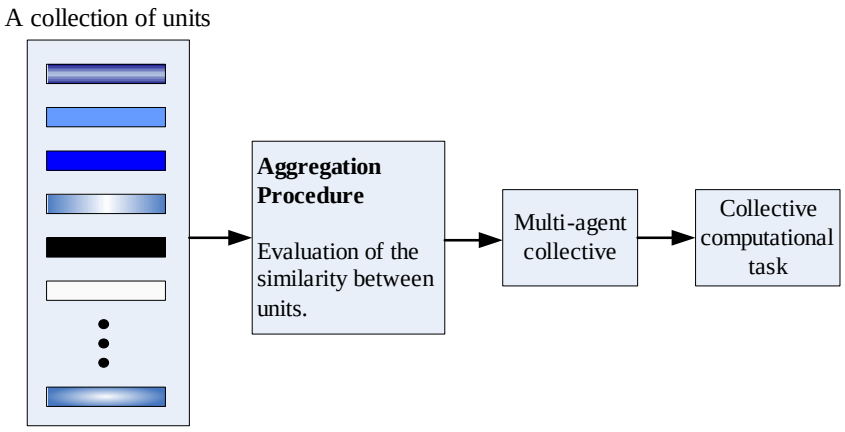

Figure 3-2: Overview of the formation of multi-agent collectives developed in this research.

3.2.1 Aggregation Procedure

The recognition of patterns created by all units in a system under a specific setting leads to the formation of a multi-agent collective. The patterns can be understood as the re-arrangement of units within the system, so that similar units are grouped together. Referring to Figure 3-1, the patterns are observed in the middle box (the *aggregated state*). The leftmost box, on the other hand, illustrates the units before they are arranged into patterns (the *original state*). The main goal of this aggregation procedure is to devise a systematic way to make the transition from the original state to the aggregated state. There are two main considerations in this transition: first, how to assess the similarity between units, or the *similarity assessment*; and second, how to form agents based on the similarity assessment results.

The similarity assessment emphasizes the interactions between units instead of properties of the individual unit. In this research, we limit the similarity assessment to consider only two units at a time. For this purpose, we need to define criteria, i.e., the *aggregation criteria*, to quantify the similarity between any two units. These aggregation criteria are used extensively in the aggregation procedure. Typically, the aggregation criteria include:

1. A quantifiable measure to express the similarity between any two units.

2. A bound or threshold value to be the passing criterion.

When the measure is below the specified threshold value, the two units are considered to be similar (*pass*); otherwise, they are not similar and, thus, not supposed to belong to the same agent (*fail*).

The formation of agents adopts the idea of the *knapsack problem* approach, which is a common approach for solving combinatorial optimization problems [7]. The name was derived from a maximization problem of choosing the optimum contents to fill a knapsack with a limited capacity. Likewise, in this procedure, an agent is formed progressively by considering an addition or subtraction of only one unit at a time.

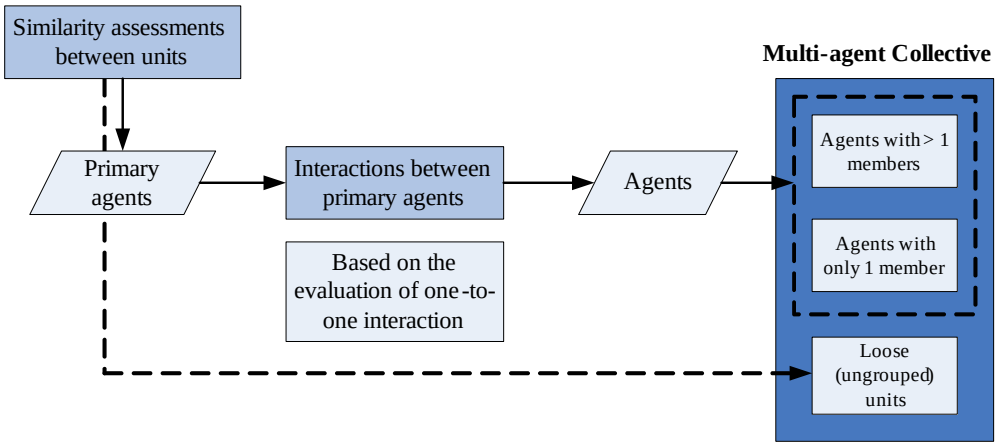

Figure 3-3: The formation of agents from units, based on the similarity assessments done on all possible pairs of units in the system.

Figure 3-3 provides an overview of steps taken to form a multi-agent collective from units. From the similarity assessment, two units that pass the aggregation criteria are considered as a *primary agent*, and they potentially belong to the same agent. Subsequently, a systematic sequence of assessments of primary agents is carried out to form the agents. This process is dynamic, in that the agents change as the process evolves. The procedure is terminated when an equilibrium is reached, i.e., when subsequent assessments no longer change the agents. For a more detailed explanation, each step in Figure 3-3 is further elaborated in Figure 3-4, and explained below.

Step 1. **Formation of Primary Agents**.

The procedure starts by examining the similarity assessments of all possible pairs of units within the system of interest. This brute-force approach is required

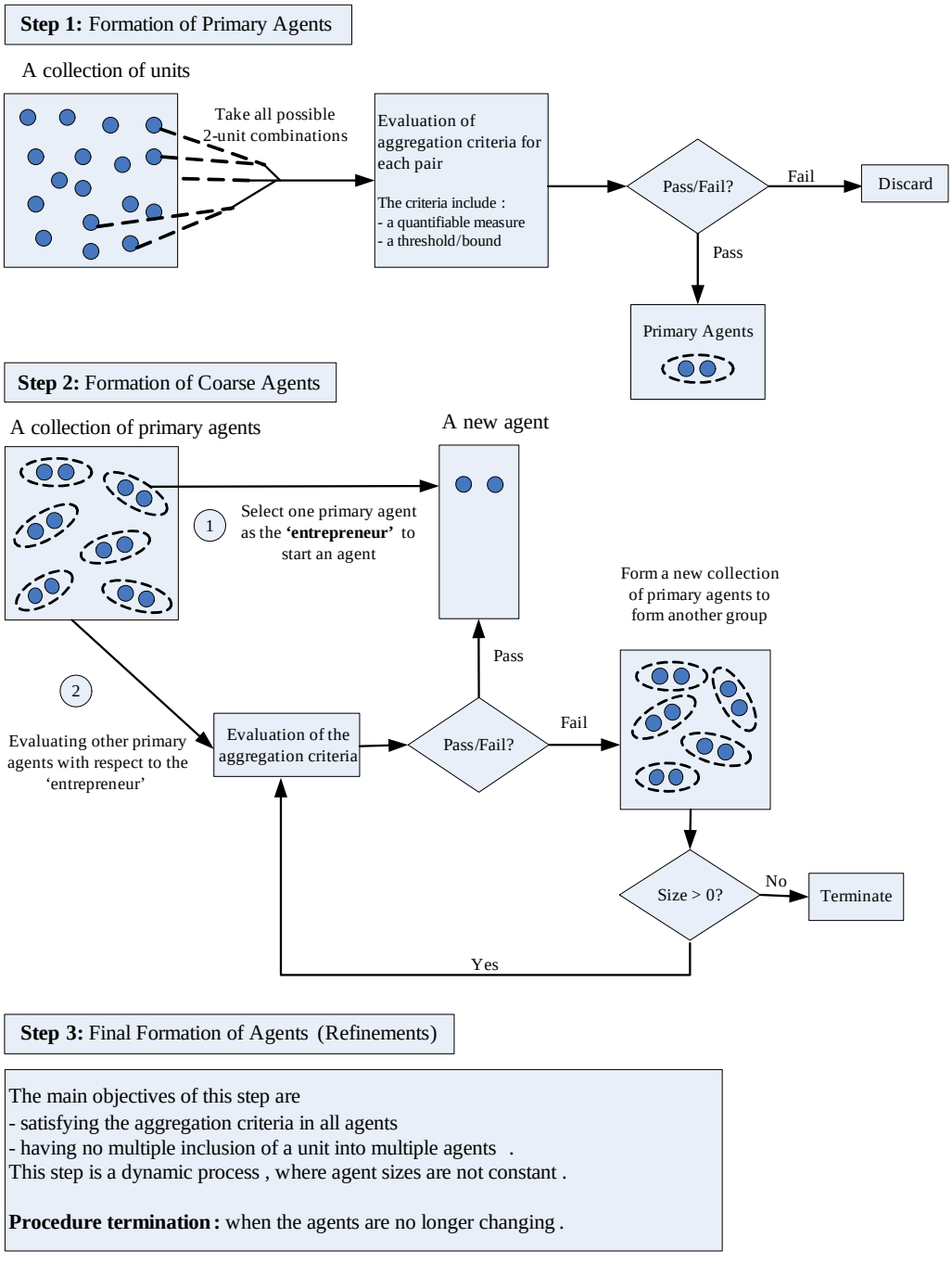

Figure 3-4: The required steps in the aggregation procedure.

for the first step due to the absence of any prior knowledge about the units and the interactions between units. The aggregation criteria are evaluated for each pair of units, and pairs that pass the criteria are considered as primary agents. Each primary agent contains only two units. This step provides a list of primary agents and a list of loose (ungrouped) units. This primary agent list forms the reference, as a look-up table, for subsequent assessments. The list of ungrouped units is stored separately and is appended to the list of agents after the agent formation has been finalized (see Figure 3-3).

Step 2. **Formation of Coarse Agents**.

At this step, the interactions between primary agents are evaluated, based only on the list of primary agents from the previous step. A primary agent is arbitrarily selected to be the *entrepreneur* to initiate a new *coarse agent*. The term coarse agent is used to indicate that the formed agent may not be the final agent. Next, the procedure searches through other primary agents in the list. A new member is added to the coarse agent when the search finds a primary agent that has a common unit with the coarse agent. The unit in that particular primary agent that is not the common unit is added to the coarse agent. The search finishes when all primary agents in the current list have been evaluated. The primary agent list is then updated by removing the primary agents that have joined the coarse agent. To form the next coarse agent, one primary agent from the updated primary agent list is selected to be an entrepreneur. This new coarse agent is formed by following the same search as before. The same procedure, to form a coarse agent, is repeated until the primary agent list is empty.

Step 3. **Final Formation of Agents (Refinements)**.

The main objective of refining the agents is to ensure that:

(a) All agents satisfy the aggregation criteria.
(b) All units must not be a member of more than one agent.

The procedure carried out in Step 2 is insufficient to ensure that the aggregation criteria are satisfied for all possible similarity assessments within an agent.

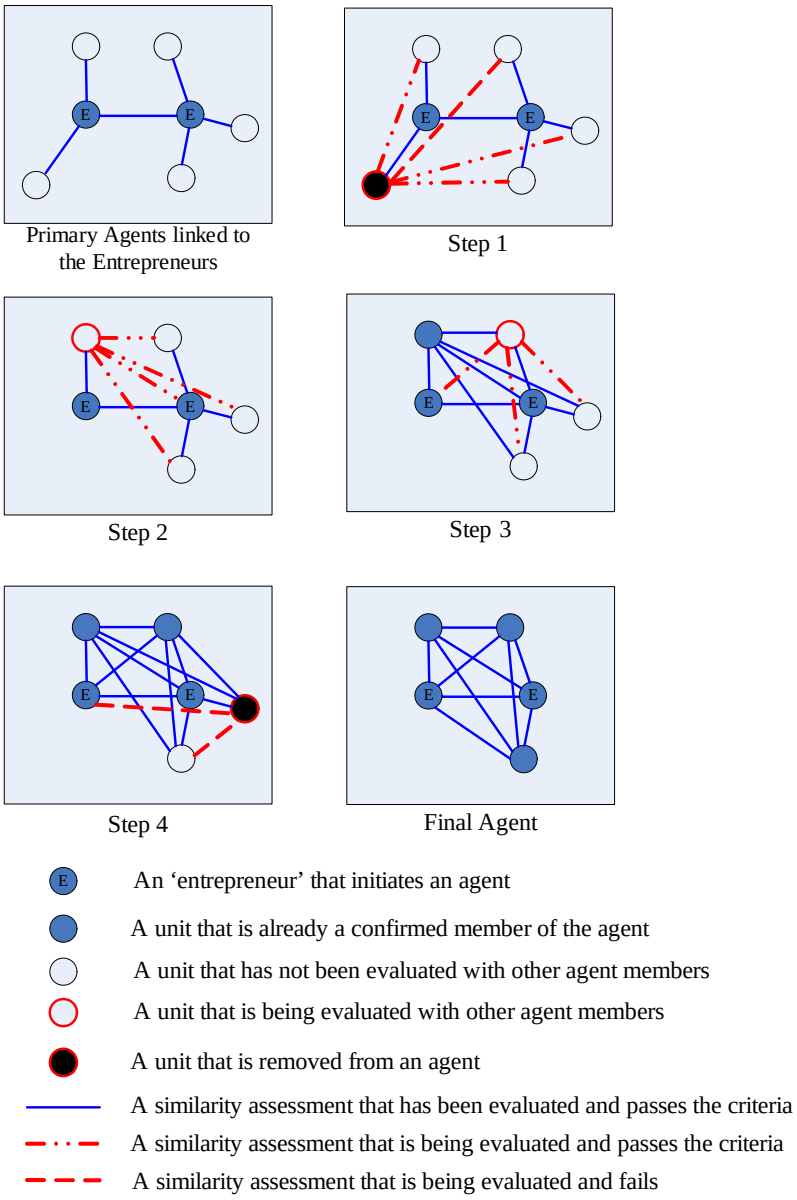

Figure 3-5: Refinements of coarse agents to ensure that the aggregation criteria are satisfied among all members in an agent.

Instead, the procedure only ensures that a unit in an agent is similar to at least one other member of the agent. Figure 3-5 illustrates a simple case where some units are removed systematically from an agent when the aggregation criteria are not satisfied. One unit is evaluated at each step by looking at its similarity assessments with all other agent members. The original primary agent list is used as the reference. A unit that has at least one similarity assessment that fails the aggregation criteria is removed from the agent. The procedure is repeated for all units, excluding the removed units.

The final assessment is done to avoid any *multiple inclusions* of a unit, i.e., when a unit is a valid member of more than one agent. The removal of such occurrences is done by analyzing two agents at a time. Agents to be analyzed are those that have common members with other agents, which will be referred to as *linked agents*. The steps taken to remove such multiple inclusions are described as follows:

(a) Find agents that have common members with other agents (linked agents).

(b) When more than two agents are *linked* together, list all possible pairings to be analyzed. For example, agents X, Y, and Z have common members. We then list all possible pairings: $[X, Y]$, $[Y, Z]$, and $[X, Z]$ and use these pairings instead to carry out the next steps.

(c) Define the following terms for each pair of linked agents:

   i. Minor agent, Mi:

      This refers to the agent, among the two, with a smaller number of members when the agent sizes are different, or an arbitrarily selected agent when agent sizes are the same.

   ii. Major agent, Ma:

      This refers to the agent that is not defined as the minor agent.

   iii. Common members, Co:

      This refers to a collection of units that belong to both minor and major agents. In a mathematical expression, we can describe it as $Co = Mi \cap Ma$.

(d) Evaluate each pair of linked agents.

There are three cases identified for this evaluation that are illustrated in Figure 3-6 and also listed below. In the figure, the colors of the major agent (Ma) indicate whether it changes or remains the same after the evaluation. When the color does not change, it means that the major agent does not change. A darker color means it has additional members, whereas a lighter color indicates that there are some members that are removed from the agent. In the explanation below, $|\cdot|$ is used to express the number of members within a set.

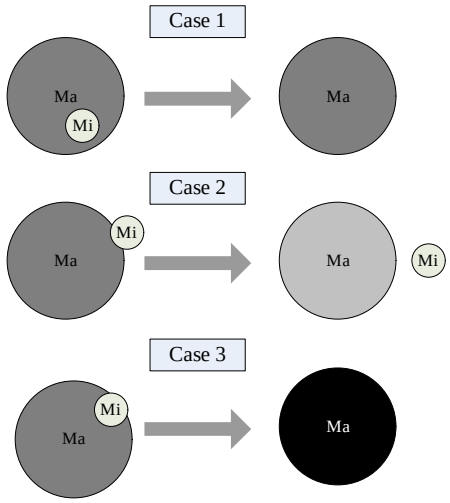

Figure 3-6: Three cases in the evaluation of each pair of linked agents.

Case 1. $Co = Mi$

Action taken: remove Mi.

Case 2. $Co \neq Mi$ and $|Co| < \frac{1}{2}|Mi|$

Action taken: remove Co from Ma, and Mi remains unchanged.

Case 3. $Co \neq Mi$ and $|Co| \geq \frac{1}{2}|Mi|$

Action taken: remove Mi and join Mi to Ma.

(e) Repeat the procedure until all multiple inclusions have been removed.

3.2.2 Distribution of the Collective Computational Task

With the formation of a multi-agent collective, the computational cost of the system can be reduced by considering the system as constructed by a number of agents, which are much fewer than the total number of units. For this purpose, a unit is selected from each agent to be the agent representative. We discussed at the beginning of this chapter that each unit is unique, even among similar units that form an agent. It is, therefore, very unlikely that the computational task performed using agent representatives gives the exact same output as when the computation is done by considering all units. An error, quantified as the discrepancy between outputs from the surrogate and full models, is expected to exist. This error determines the quality of the surrogate model, i.e., how good a surrogate model is in representing the full model. As it is desirable to minimize the error, the selection of agent representatives is one of critical consideration in the formation of a multi-agent collective, and must be done carefully. The particular strategy used to select agent representatives will depend on the problem at hand. In the next chapter, we present application of the surrogate modeling method to a case study that estimates the fuel burn of the global aircraft fleet. In that context we discuss further details of the method, such as a strategy for selecting agent representatives.

Chapter 4

Surrogate Modeling for Fuel Burn Estimation

This chapter presents the demonstration of the developed surrogate modeling method, applied to the fuel burn estimation model within APMT. The chapter begins by describing the implementation of the developed method for this specific case. The surrogate model derived based on SAGE Flight Inventory from 2005 (Ξ_{2005}) is then presented and discussed.

In [34], Lee selected a small number of aircraft types to represent the aircraft performance characteristics in the full SAGE fleet including 359 aircraft types. 11 aircraft types of a major US carrier were selected and Monte Carlo simulations were carried out to study the difference between nominal fuel burn and mean fuel burn. The mean of the computed errors in that study is -4.4% with a standard deviation of 16.0%. It has also been shown in the study that on average, uncertainties contribute to a difference between estimated and reported fuel burn of approximately 6%. Some most influential uncertainties in the study include the atmospheric conditions, aerodynamic and engine performance, aircraft take-off weight, flight speed, and the Official Airline Guide (OAG)-based flight trajectories. Therefore a surrogate modeling error of 6% is deemed acceptable in the context of the computation of fuel burn estimates.

4.1 Multi-Agent Collective Formation

Table 4.1 summarizes the implementation of surrogate modeling procedure for estimation of fuel burn. Each of the steps—the selection of the aggregation unit, the computation of

fuel burn for each unit, and the method to perform similarity assessments between units—is then described in detail. Following these descriptions, the implementation of aggregation procedure to derive the surrogate model is presented.

Surrogate Modeling Component	**Specification for fuel burn estimation example**
Aggregation unit	Aircraft type.
Fuel burn computation for each unit	A functional approximation by a linear regression analysis performed on cruise fuel burn and cruise distance.
Aggregation criteria	Cross-estimation error, ε_c, and a threshold value, δ_t.
Similarity assessments	Evaluation of cross-estimation errors between any two units. The gradient ratio, γ (Equation 4.15), is used as the *a priori* cross-estimation error approximation.
Aggregation procedure	Formation of primary and coarse agents (Figure 4-3), continued by the finalization (refinements) of agents (Figure 4-4).
Selection of the agent representative	An aircraft type that travels the maximum total distance within an agent is selected to be the agent representative.

Table 4.1: Summary of the surrogate modeling procedure for fuel burn aggregation.

4.1.1 Selection of the Aggregation Unit

Selection of the appropriate aggregation unit is crucial to form an effective multi-agent collective. A unit, as described in Chapter 3, has to be unique and distinguishable from other units. In this case study, the aggregation unit is selected by considering the fuel burn computation method in SAGE. The method, as presented in Chapter 2, suggests that aircraft type is a suitable metric by which we can differentiate the fuel burn computation of one flight from another. Factors that are specific to an aircraft type, such as BADA coefficients, aircraft wing area, and aircraft mass, account for the distinct fuel burn computation. Fur-

ther, the data sets used in this research are organized so as to permit classification of flights based on aircraft type. Thus, in this case study, an aircraft type is used as the aggregation unit.

The following surrogate modeling procedure groups similar aircraft types together, where each group is referred to as an agent. The selection of a representative aircraft type from each agent enables the simplification of the original system to a multi-agent collective, with which the computation of total fuel burn estimates will be performed.

4.1.2 Collective Computational Task

A fuel burn computation, corresponding to each aircraft type, is required to assess the surrogate model created by this procedure. The limited flight information in the data sets that are used in this research prohibits the implementation of the fuel burn computation method employed in SAGE. Thus, we explore a functional approximation, which is derived from the available flight data, to compute the total fuel burn estimates, that is, the fuel burned over an entire year of flight operations, corresponding to each aircraft type. The amount of fuel burned during a flight increases as the flight travels a greater distance, as also shown in Figure 4-1. The flight data plotted in the figure correspond to an arbitrarily selected aircraft type (A319), from two data sets, i.e., Ξ_{CFDR} and Ξ_{2005}. A line fit is also displayed on each plot, assuming a linear relationship between fuel burn and flight distance. The plots exhibit that the relationship between fuel burn and flight distance can be approximated by a linear function.

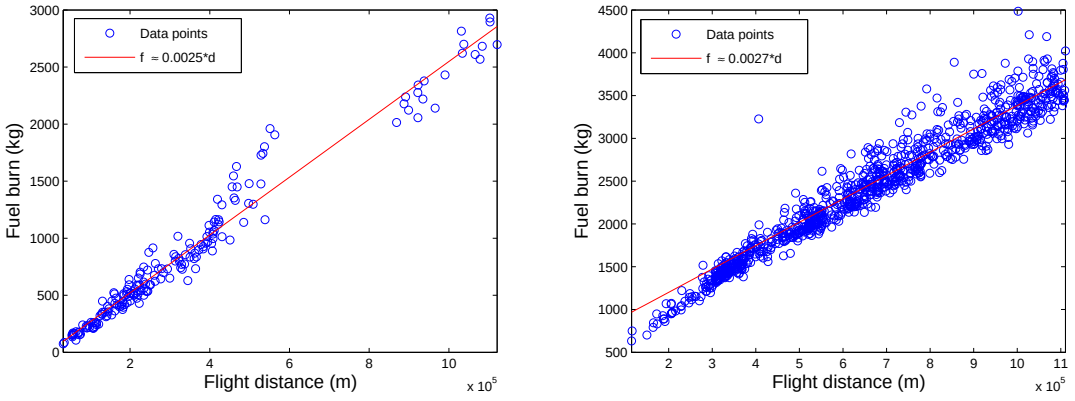

(a) with data from Ξ_{CFDR}

(b) with data from Ξ_{2005}

Figure 4-1: Fuel burn vs flight distance plots with A319 aircraft type.

To provide the functional approximation for the fuel burn and distance relationship, a linear regression analysis is performed on the available cruise distance and cruise fuel burn data for each aircraft type. The linear equation for each flight can be expressed as

$$f_{i\,j} = \beta_{1\,j} \cdot d_{i\,j} + \beta_{0\,j} + \varepsilon_{i\,j}, \tag{4.1}$$

where i denotes the flight index within an aircraft type and j denotes the index of aircraft type within a data set. $\beta_{0\,j}$ and $\beta_{1\,j}$ are the regression parameters, and $\varepsilon_{i\,j}$ is the error term for a specific flight, i.e., the discrepancy between the linear approximation of fuel burn (which is denoted as $\tilde{f}_{i\,j}$) and the actual fuel burn ($f_{i\,j}$). We use the method of least squares to find the values of $\beta_{0\,j}$ and $\beta_{1\,j}$ that minimize the summation of the squares of deviation of $f_{i\,j}$ from $\tilde{f}_{i\,j}$, over all flights i. The selected regression parameters for a specific aircraft type are referred to as $b_{0\,j}$ and $b_{1\,j}$. Mathematically, we express the minimization problem for aircraft type j in Equation 4.2,

$$(b_{0\,j}, b_{1\,j}) = \arg \min_{\beta_{0\,j}, \beta_{1\,j}} \sum_{i=1}^{N_{f\,j}} (f_{i\,j} - \beta_{1\,j} \cdot d_{i\,j} - \beta_{0\,j})^2, \tag{4.2}$$

where $N_{f\,j}$ denotes the number of flights of the j-th aircraft type. Let $G(\beta_{0\,j}, \beta_{1\,j})$ be the sum of squared errors over all flights within an aircraft type or,

$$G(\beta_{0\,j}, \beta_{1\,j}) = \sum_{i=1}^{N_{f\,j}} (f_{i\,j} - \beta_{1\,j} \cdot d_{i\,j} - \beta_{0\,j})^2 \Rightarrow G(\beta_{0\,j}, \beta_{1\,j}) = \sum_{i=1}^{N_{f\,j}} \left(f_{i\,j} - \tilde{f}_{i\,j}\right)^2. \tag{4.3}$$

As $b_{0\,j}$ and $b_{1\,j}$ are the minimizers for $G(\beta_{0\,j}, \beta_{1\,j})$, the following condition must be satisfied for all j:

$$\frac{\partial G(b_{0\,j}, b_{1\,j})}{\partial b_{0\,j}} = 0 \Rightarrow -2 \cdot \sum_{i=1}^{N_{f\,j}} \left(f_{i\,j} - \tilde{f}_{i\,j}\right) = 0 \Rightarrow \sum_{i=1}^{N_{f\,j}} f_{i\,j} = \sum_{i=1}^{N_{f\,j}} \tilde{f}_{i\,j}. \tag{4.4}$$

Equation 4.4 shows that the total fuel burn for one aircraft type can be obtained exactly from the summation of all estimates ($\tilde{f}_{i\,j}$, $\forall i$), although each estimate is unable to give the exact fuel burn value, i.e., $\tilde{f}_{i\,j} \neq f_{i\,j}$. Thus, the total fuel burn for an aircraft type, $\mathbf{f}_j$, can be expressed as

$$\mathbf{f}_j = \sum_{i=1}^{N_{f\,j}} f_{i\,j} \Rightarrow \mathbf{f}_j = b_{1\,j} \cdot \sum_{i=1}^{N_{f\,j}} d_{i\,j} + N_{f\,j} \cdot b_{0\,j}. \tag{4.5}$$

The observation in Equation 4.5 leads to a significant computational cost reduction in estimating total fuel burn, as the fuel burn computation for each flight is no longer required. Instead, the equation obtained from the linear regression analysis per aircraft type is employed to compute the total fuel burn for that particular aircraft type.

4.1.3 Similarity Assessment

The next step in the surrogate modeling procedure is to derive the aggregation criteria to assess the similarity between any two units. The aggregation criteria comprise a quantifiable measure and a threshold value to define whether the two units pass, in which case the two units can become a primary agent, or fail. Specifically in the context of this case study, we specify that two units pass the aggregation criteria if the linear regression equation of one aircraft type can be used to estimate the total fuel burn of the other aircraft type, within a specified accuracy. This accuracy becomes the threshold value, denoted by δ_t. In this thesis, the process of estimating the fuel burn of one aircraft type by the linear regression equation of another aircraft type is referred to as a *cross-estimation*. Correspondingly, the error associated with the process is called the *cross-estimation error*, which is used to quantify the similarity between any two units. In a cross-estimation, we differentiate the two following roles for the two aircraft types:

Role 1. Reference aircraft type.

A reference aircraft type is the aircraft type whose linear regression equation is used to estimate the total fuel burn of the other aircraft type.

Role 2. Test aircraft type.

A test aircraft type is the aircraft type whose total fuel burn is estimated by the linear regression equation of the reference aircraft type.

In this context, we define the *reversal role* of a cross-estimation as another cross-estimation that involves the same pair of aircraft types, but with exchanged roles. The formation of primary agents requires two steps, namely:

Step 1. Formation of *potential primary agents*.

The potential primary agents include pairs of a reference and a test aircraft type that yield cross-estimation errors below the specified threshold value or,

$$|\varepsilon_c| \leq \delta_t, \tag{4.6}$$

where ε_c is the cross-estimation error.

Step 2. Formation of primary agents.

To form the primary agents, pairs whose reversal roles are also included in the list of potential primary agents are selected. In other words, the two possible cross-estimations in a primary agent must satisfy Equation 4.6.

An *a priori* cross-estimation error approximation is derived to eliminate the need to compute the total fuel burn of the test aircraft type, using the linear regression equation of the reference aircraft type, at each cross-estimation. First, we define the notations used in the linear regression analysis for reference aircraft type (denoted by the index r),

$$\mathbf{f}_r = b_{1\,r} \cdot \sum_{i=1}^{N_{f\,r}} d_{i\,r} + N_{f\,r} \cdot b_{0\,r}, \tag{4.7}$$

and similar analysis for test aircraft type (denoted by the index t),

$$\mathbf{f}_t = b_{1\,t} \cdot \sum_{i=1}^{N_{f\,t}} d_{i\,t} + N_{f\,t} \cdot b_{0\,t}. \tag{4.8}$$

The estimated fuel burn from cross-estimation, $\tilde{\mathbf{f}}_t$, is then computed by Equation 4.9,

$$\tilde{\mathbf{f}}_t = b_{1\,r} \cdot \sum_{i=1}^{N_{f\,t}} d_{i\,t} + N_{f\,t} \cdot b_{0\,r}. \tag{4.9}$$

The cross-estimation error (ε_c) is expressed as

$$\varepsilon_c = \frac{\tilde{\mathbf{f}}_t - \mathbf{f}_t}{\mathbf{f}_t} \cdot 100\%. \tag{4.10}$$

From Equations 4.7 to 4.10, the following equation is obtained,

$$\varepsilon_c = \frac{\left(b_{1\,r} \cdot \sum_{i=1}^{N_{f\,t}} d_{i\,t} + N_{f\,t} \cdot b_{0\,r}\right) - \left(b_{1\,t} \cdot \sum_{i=1}^{N_{f\,t}} d_{i\,t} + N_{f\,t} \cdot b_{0\,t}\right)}{b_{1\,t} \cdot \sum_{i=1}^{N_{f\,t}} d_{i\,t} + N_{f\,t} \cdot b_{0\,t}} \cdot 100\%.$$

After rearranging, the above equation becomes

$$\varepsilon_c = \left(\frac{(b_{1\,r} - b_{1\,t}) \cdot \sum_{i=1}^{N_{f\,t}} d_{i\,t}}{b_{1\,t} \cdot \sum_{i=1}^{N_{f\,t}} d_{i\,t} + N_{f\,t} \cdot b_{0\,t}} + \frac{(b_{0\,r} - b_{0\,t}) \cdot N_{f\,t}}{b_{1\,t} \cdot \sum_{i=1}^{N_{f\,t}} d_{i\,t} + N_{f\,t} \cdot b_{0\,t}}\right) \cdot 100\%. \tag{4.11}$$

For simplicity, let:

$$z = \frac{N_{f\,t}}{\sum_{i=1}^{N_{f\,t}} d_{i\,t}}. \tag{4.12}$$

Substituting Equation 4.12 into Equation 4.11,

$$\varepsilon_c = \left(\frac{b_{1\,r} - b_{1\,t}}{b_{1\,t} + b_{0\,t} \cdot z} + \frac{b_{0\,r} - b_{0\,t}}{\frac{b_{1\,t}}{z} + b_{0\,t}}\right) \cdot 100\%$$

$$\Rightarrow \varepsilon_c = \frac{\left(b_{1\,r} \cdot b_{1\,t} - {b_{1\,t}}^2\right) + \left(b_{1\,r} \cdot b_{0\,t} - 2 \cdot b_{1\,t} \cdot b_{0\,t} + b_{0\,r} \cdot b_{1\,t}\right) \cdot z + \left(b_{0\,r} \cdot b_{0\,t} - b_{0\,t}\right) \cdot z^2}{{b_{1\,t}}^2 + 2 \cdot b_{1\,t} \cdot b_{0\,t} \cdot z + {b_{0\,t}}^2 \cdot z^2} \cdot 100\%. \tag{4.13}$$

The notation z refers to the inverse of average flight distance for a particular aircraft type. We assume that z is very small and, thus, Equation 4.13 can be simplified to the following by only considering the dominant terms,

$$\varepsilon_c \approx \frac{b_{1\,r} - b_{1\,t}}{b_{1\,t}} \cdot 100\%. \tag{4.14}$$

To validate this assumption, Equation 4.14 is computed for all possible pairs of aircraft types within Ξ_{2005}. The pairs where the computed values fall between -100% and 500% are selected. Figure 4-2 displays the actual cross-estimation errors corresponding to the selected pairs plotted against the values computed by Equation 4.14. The figure shows the plots of 6400 data points pertaining to pairs of a reference and a test aircraft type. The slope of the relationship between the computed value and the corresponding cross-estimation error is computed to be 0.97. From the computation of the coefficient of determination, R^2, this linear regression is shown to account for 96.40% of variability in the data set. Based on

these analyses, we conclude that the earlier assumption is valid. Thus, we define a gradient ratio, (γ), to be the *a priori* cross-estimation error approximation for this case study. The computation of the gradient ratio is given in Equation 4.15,

$$\gamma = \frac{\Delta b_1}{b_{1\,t}} \cdot 100\%. \tag{4.15}$$

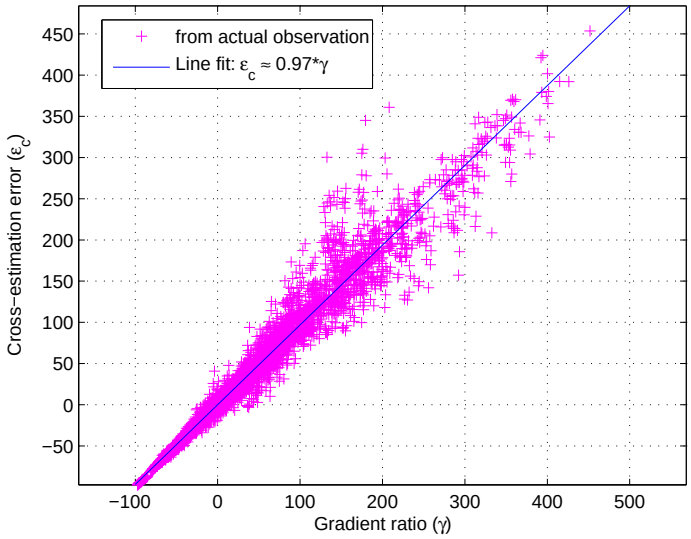

Figure 4-2: The plot of cross-estimation error (ε_c) against the value computed by Equation 4.14 when the computed value is within the range of -100% and 500%.

4.1.4 Aggregation Procedure

The general aggregation procedure is illustrated in Figure 3-4; however, in this case study we define a potential primary agent, in addition to the primary agent. The implementation of the algorithm in this case study is illustrated in Figure 4-3, which summarizes Step 1 and 2 of the aggregation procedure. This figure first presents the formation of potential primary agents, followed by the formation of primary agents. The coarse agents are then formed from the list of primary agents, following the knapsack problem approach, as described in Chapter 3. Figure 4-4 provides the implementation of Step 3, where the agents are finalized by first identifying the linked agents, as also described in the previous chapter. At the end of this procedure, all possible pairs of aircraft type within an agent satisfy the aggregation criteria, and it is also ensured that each aircraft type is a valid member of only one agent,

i.e., there are no multiple inclusions.

4.1.5 Distribution of the Collective Computational Task

The distribution of the collective computational task is carried out by selecting a representative from each agent. That is, the total fuel burn for all aircraft types within an agent, $\tilde{\mathbf{f}}_{a\,k}$, is computed by using the linear regression equation of the selected representative aircraft type, by taking all flights within an agent into account. This computation is expressed as

$$\tilde{\mathbf{f}}_{a\,k} = b_{1\,k} \cdot \sum_{j \in A_k} \sum_{i=1}^{N_{f\,j}} d_{i\,j} + b_{0\,k} \cdot \sum_{j \in A_k} N_{f\,j}, \tag{4.16}$$

where $b_{0\,k}$ and $b_{1\,k}$ are the regression parameters corresponding to the k-th agent's representative aircraft type, and A_k denotes a set of aircraft types that belong to the k-th agent. A representative aircraft type must be able to minimize the estimation error within an agent. It is also desirable to have a simple procedure to select the representatives. Referring to Equation 4.16, the main factor in determining the total fuel burn, when a linear regression equation is used, is the total flight distance. Therefore, the aircraft type within the agent of interest that traveled the maximum total distance is selected to be the agent representative.

Figure 4-5 provides an overview of the expected computational cost reduction gained by forming the surrogate model. In the figure, N_{AC} refers to the total number of aircraft types included in the data set, and N_{agent} refers to the total number of agents formed by the surrogate modeling method. The computational cost reduction is summarized as follows:

1. Reduction of the required computations by eliminating the need to compute the fuel burn for each flight.

   Instead, the total fuel burn for all flights within an aircraft type is computed using the linear regression equation derived for the specific aircraft type. Thus, the total number of fuel burn computations required equals to the total number of aircraft types within the system.

2. Reduction of the required computations by selecting agent representatives.

   As the fuel burn computation for each agent is done by employing Equation 4.16, the number of computations required is further reduced to the number of formed agents.

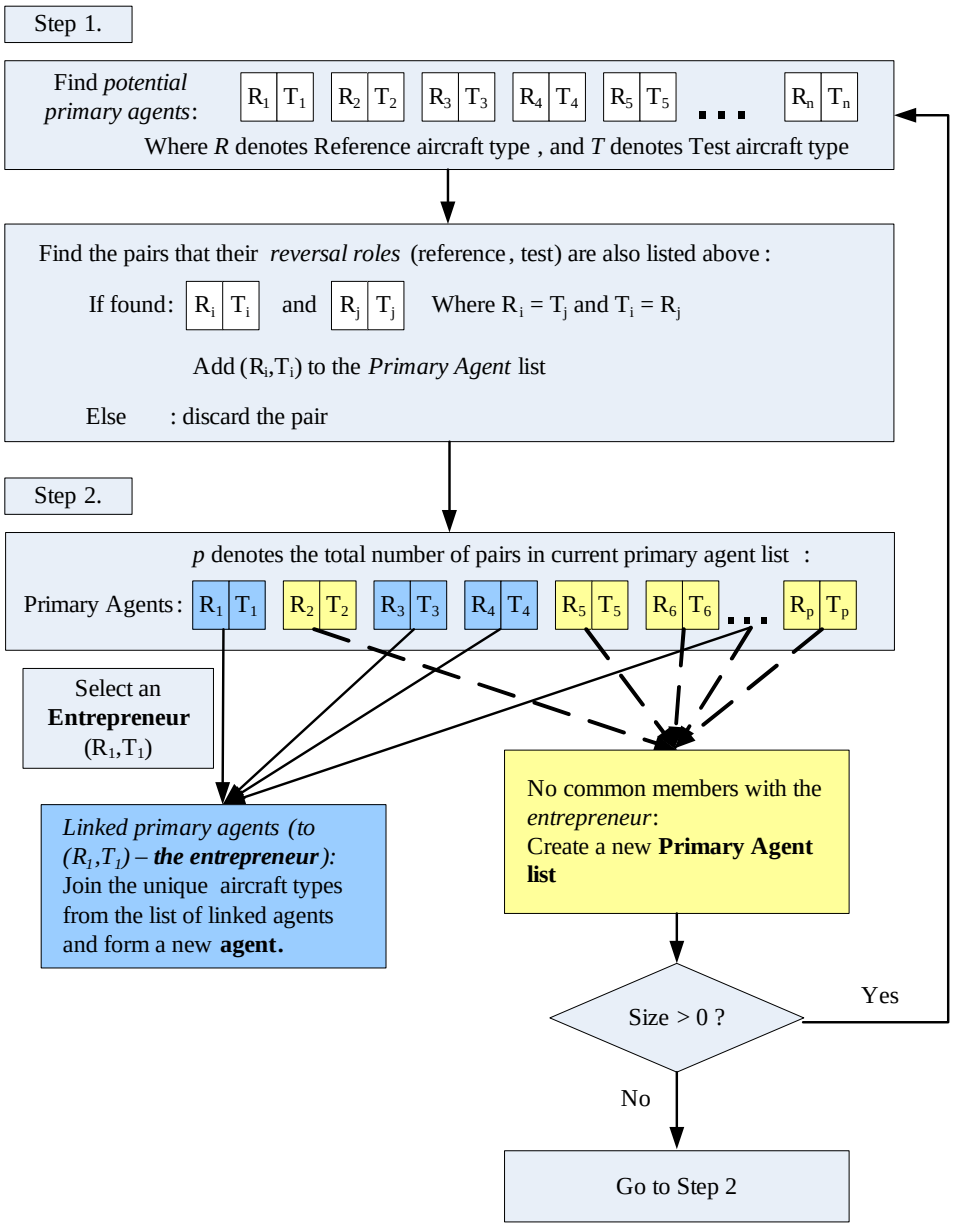

Figure 4-3: Step 1 and 2 of the aggregation procedure (Figure 3-4): The flowchart for the formation of coarse agents in the total fuel burn estimation case study.

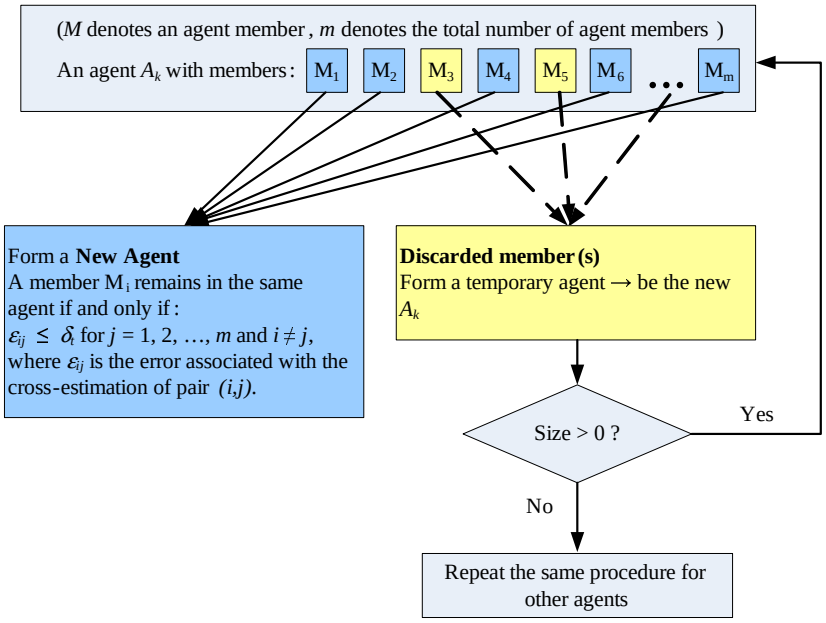

Figure 4-4: Step 3 of the aggregation procedure (Figure 3-4): The flowchart for the refinements of coarse agents in the total fuel burn estimation case study.

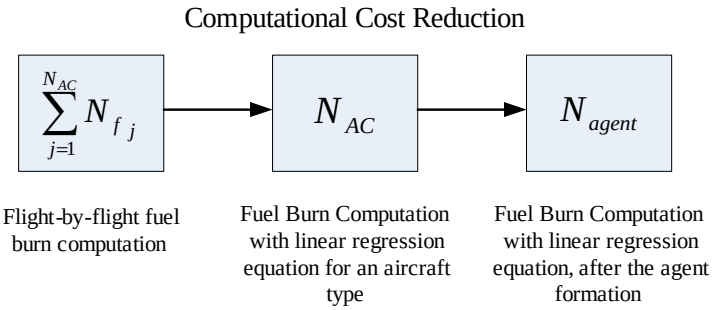

Figure 4-5: Computational cost reduction of total fuel burn estimation.

Based on the above discussion, the following must be true for the surrogate model to be effective,

$$\sum_{j=1}^{N_{AC}} N_{f\,j} \lll N_{AC} \ll N_{agent}.$$

To rate the performance of agents, we use the *total estimation error*, ε, that measures the discrepancy between total fuel burn computed by agents and the actual total fuel burn. The total estimation error is expressed in Equation 4.17,

$$\varepsilon = \frac{\sum_{k=1}^{N_{agent}} \tilde{\mathbf{f}}_{a\,k} - \sum_{j=1}^{N_{AC}} \mathbf{f}_j}{\sum_{j=1}^{N_{AC}} \mathbf{f}_j} \cdot 100\%. \tag{4.17}$$

4.2 Results

The surrogate model derived based on Ξ_{2005} and the corresponding total estimation errors are presented first in this section. Next, the results of application of the surrogate model to other SAGE Flight Inventory data sets, for validation purposes, are discussed. Lastly, a comparison is made between the developed surrogate model and a *manual aggregation*, that is, when the aggregation of aircraft types is done manually based on engineering knowledge of aircraft types.

4.2.1 The Surrogate Model

We consider two competing objectives in the multi-agent collective formation: total estimation error and number of agents. It is always desirable that the surrogate model is able to yield a low total estimation error. At the same time, the number of agents formed needs to be much fewer than the number of aircraft types, in order to gain a significant computational cost reduction. There is a natural tradeoff between these two aspects, which, in this research, is adjusted by controlling the threshold value, δ_t.

The variations of total estimation errors and numbers of agent with threshold values are plotted in Figure 4-6. As an analytical relationship between the threshold value and total estimation error is unavailable, the threshold value is selected by applying a simple search

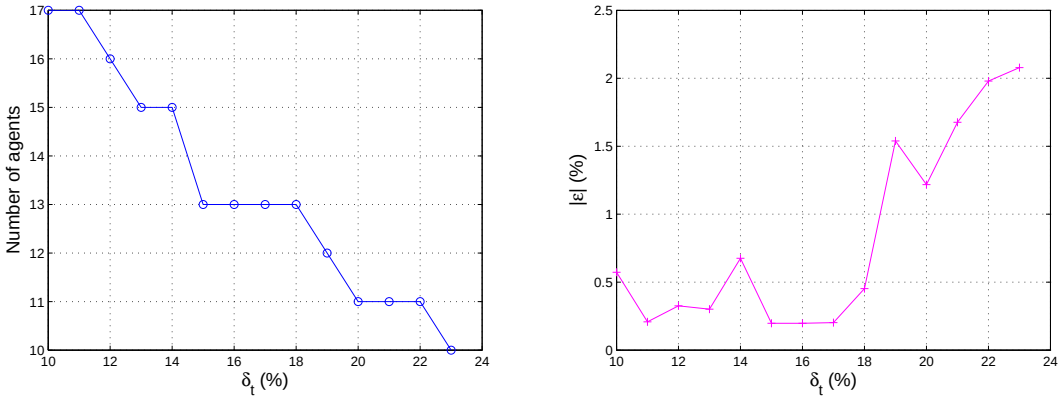

(a) Variation of number of agents

(b) Variation of $|\varepsilon|$

Figure 4-6: The variation of number of agents and estimation error with varying threshold value.

procedure. The search starts from a threshold value of 10%, which is arbitrarily selected, with a 1% increment at each search step. For this case, the search terminates when one of the following condition occurs: (a) the estimation error is greater than 5%, or (b) the number of agents is less than or equal to ten. With Ξ_{2005} data, the search terminates when a threshold value of 23% is reached. The number of agents formed by the procedure is ten, with a corresponding total estimation error of 2.08%. Table 4.2 tabulates the ten agents formed by the procedure; the selected agent representatives are typed in bold. The descriptions of the aircraft types shown in the table are given in Appendix A.

From Figure 4-6 (a), we observe that the number of agents decreases with increasing threshold value. This is an expected outcome, as increasing threshold value reduces the stringency of the similarity assessment. The estimation errors plotted in Figure 4-6 (b) do not exhibit any distinct trends, although the total estimation errors tend to increase with increasing threshold values. This behavior, however, is not consistently observed throughout all threshold values, for example between 14% and 15%. To further observe the variation of total estimation errors, the distribution of estimation errors corresponding to individual agents is studied. This individual agent's estimation error is denoted as ε_k, with k referring to the index of an agent, and expressed as

Agent No.	Members of Agents
1	A300, A30B, A306, A308, A332, A340, A342, **A343**, A345, A346, B701, L101, IL62
2	A310, A330, A333, B762, **B763**, B764, B767, DC8, DC85, DC86, DC87, DC8Q, T154
3	B703, **B772**, B773, B777, DC10, MD11
4	A321, B727, **B752**, B753, B754, B757, YK40, YK42, MD80, MD81, MD82, MD83, MD87, MD88, MD90, T204
5	**B741**, B743, B74R, B74S
6	**DC9**, F100, TU34
7	A318, A319, **A320**, B462, B712, B717, B732, B733, B734, B736, B737, B738, B739, B73A, B73B, B73Q, B73S, DC91, DC92, DC93, DC94, DC95, DC9Q
8	B742, **B744**
9	**N260**
10	**T34T**

Table 4.2: The multi-agent collective derived based on Ξ_{2005} with threshold value $\delta_t = 23\%$. Total number of agents is 10 and the total estimation error is 2.08%.

$$\varepsilon_k = \frac{\tilde{\mathbf{f}}_{a\,k} - \sum_{j \in A_k} \mathbf{f}_j}{\sum_{j \in A_k} \mathbf{f}_j} \cdot 100\%. \tag{4.18}$$

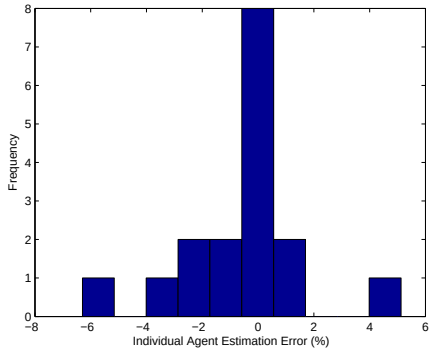

(a) Minimum error #1, $\delta_t = 11\%$. Mean = - 0.63%, $\sigma = 2.31\%$.

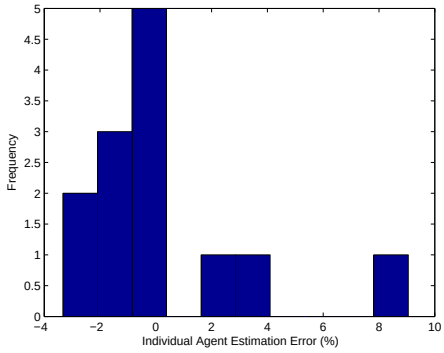

(b) Minimum error #2, $\delta_t = 15\%$. Mean = 0.30%, $\sigma = 3.20\%$.

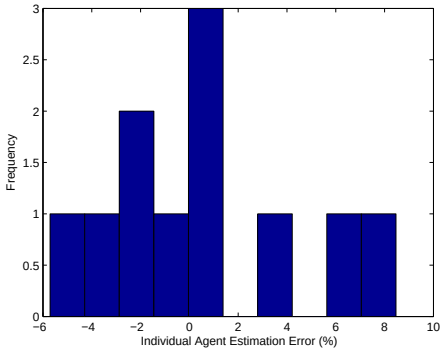

(c) Maximum error #1, $\delta_t = 22\%$. Mean = 0.54%, $\sigma = 4.17\%$.

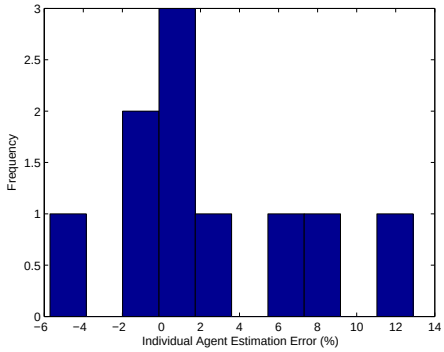

(d) Maximum error #2, $\delta_t = 23\%$. Mean = 2.31%, $\sigma = 5.52\%$.

Figure 4-7: Four distributions of individual agents' estimation errors for fuel burn computation: two threshold values have maximum total estimation errors, and the other two have minimum total estimation errors.

The distribution of individual agents' estimation errors (ε_k, $\forall k$) are displayed in Figure 4-7 for four threshold values: two threshold values that yield the maximum total estimation errors (refer to Figure 4-6) and two threshold values that correspond to the minimum total estimation errors. In the figure, the mean and standard deviation for each individual agent's estimation error distribution are also shown. A few observations can be made from the figure, and are discussed in the following.

1. The computed maximum individual agent's estimation error is 12.89%, which is ob-

served when a threshold value of 23% is used. This threshold value corresponds to the maximum total estimation error in the analysis.

2. Surrogate models that have a large total estimation error tend to have a large standard deviation in the distribution of individual agents' estimation errors.

3. The maximum absolute value of individual agent's estimation error tends to increase with increasing threshold value. This observation suggests that the threshold value is able to control the selection of agent members that, in turn, control the agent's estimation error.

4. The computed total estimation error is always lower than the maximum absolute individual agent's estimation error at a given threshold value, as displayed in Figure 4-8. This observation suggests that the fuel burn estimation performs better at the aggregated level, i.e., considering the total estimation error, than at the agent level, i.e., considering the individual agent's estimation error. There exist agents that overestimate the fuel burn computation and some others that underestimate it. These variations may cancel each other out, accounting for the better performance of fuel burn estimation at the aggregated level.

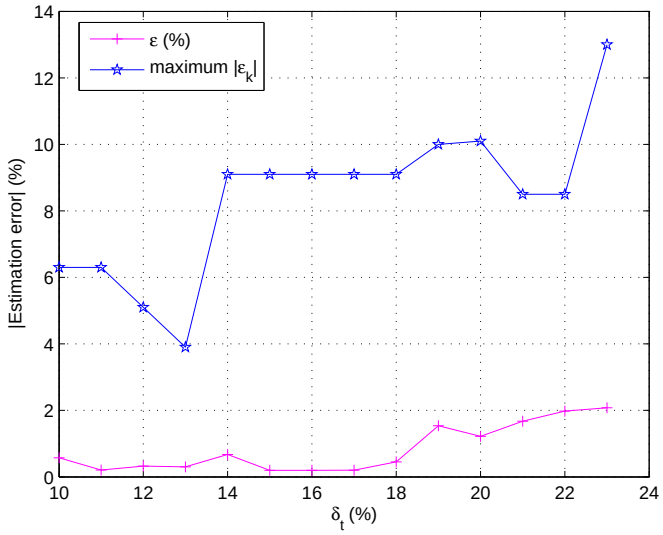

Figure 4-8: Comparison between the computed total estimation errors and the maximum absolute values of individual agents' estimation errors at various threshold values.

4.2.2 Surrogate Model Assessment

The assessment of the surrogate model is performed by applying the multi-agent collective derived based on Ξ_{2005} to other SAGE Flight Inventory data sets (Ξ_{2000} through Ξ_{2004}). The number of aircraft types included in these data sets varies, as tabulated in Table 2.3. Table 4.3 lists the aircraft types that are included in Ξ_{2005} but have no flights recorded in other data sets, referred to as *empty units* in the table.

Data sets	Empty units
Ξ_{2000}	A345, A346, DC92, T204
Ξ_{2001}	A345, A346, DC92
Ξ_{2002}	B703, B764

Table 4.3: List of aircraft types that are included in Ξ_{2005} but have no flights recorded in other data sets.

The computed total estimation errors are presented in Figure 4-9. The maximum absolute total estimation error is 2.1%, as shown in the figure. This error is deemed acceptable, based on the accuracy requirements for the surrogate model stated at the beginning of this chapter. In addition, similar trends are observed in the total estimation error plots for Ξ_{2000} through Ξ_{2005}, although some differences are also observed. Some possible causes for these variations are the different number of aircraft types within data sets and different distribution of flights amongst the aircraft types. Based on these errors, we conclude that the surrogate model derived based on Ξ_{2005} is applicable to other data sets. In other words, the aircraft types that are selected to represent Ξ_{2005} are also able to represent Ξ_{2000} through Ξ_{2004}.

One implication of this finding is that for this problem, the formation of a multi-agent collective can be done in an *offline stage*, where the procedure only needs to be performed once for a particular system. The total fuel burn estimates can then be done repeatedly, for different systems, in an *online stage* using the derived surrogate model. Nonetheless, these systems must have a setting similar to the system for which the surrogate model was derived. In our case, for example, new surrogate models may need to be derived when some assumptions in the computation are changed, e.g., International Standard Atmosphere (ISA).

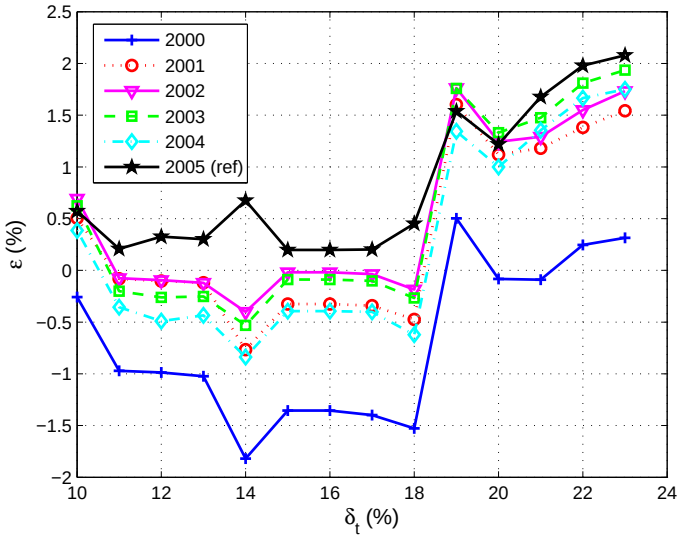

Figure 4-9: Total estimation error vs threshold value plots for Ξ_{2000}, Ξ_{2001}, Ξ_{2002}, Ξ_{2003}, Ξ_{2004}, and Ξ_{2005} by applying multi-agent collective based on Ξ_{2005}.

4.2.3 Manual Aggregation Comparison

For this problem, knowledge of the physical properties of different aircraft types enables the formation of a multi-agent collective manually. Here, the manual aggregation is performed by using engineering judgment, and specifically by considering aircraft characteristics, such as Maximum Take-off Weight (MTOW), aircraft and wing geometry, maximum cruising speed, and operating empty weight. Such an aggregation provides us with agents tabulated in Table 4.4. With this surrogate model, the estimation of total fuel burn for flights in Ξ_{2005} data set yields an error of 3.25%. Similar manual aggregation procedures have previously been explored for aircraft fuel burn and emissions analyses purposes. See, for example, [37] for a procedure to select representative aircraft types for such analyses.

The comparison between surrogate models derived from the two different aggregation methods is illustrated in Figure 4-10. The agents that are obtained from the manual aggregation are identified by the clustering of distinct aircraft types together (*spatial mapping*). The color assignments distinguish agents obtained from the surrogate modeling method (*color mapping*). Three distinct observations that can be concluded from Figure 4-10 are presented in the following.

1. Similar aggregation patterns from the two procedures.

Agent #	Members of Agents
1	A300, A30B, **A306**, A308
2	A310, A318, **A319**
3	**A320**, A321, A330, A332, A333
4	A340, A342, **A343**, A345, A346
5	**B462**
6	**B701**, B703
7	**B712**
8	B732, B733, B734, B736, B737, **B738**, B739, B73A, B73B, B73Q, B73S
9	B741, B742, B743, **B744**, B74R, B74S
10	**B752**, B753, B754, B757
11	B762, **B763**, B764, B767
12	**B772**, B773, B777
13	DC8, **DC85**, DC86, DC87, DC8Q
14	B717, DC9, DC91, DC92, DC93, DC94, DC95, DC9Q, **MD80**, MD81, MD82, MD83, MD87, MD88, MD90
15	B727, **T154**, YK42
16	DC10, L101, **MD11**
17	T34T, **TU34**
18	**F100**, IL62, N260, T204
19	**YK40**

Table 4.4: Agents formed by manual aggregation based on knowledge of aircraft types, the representative aircraft type is typed in bold.

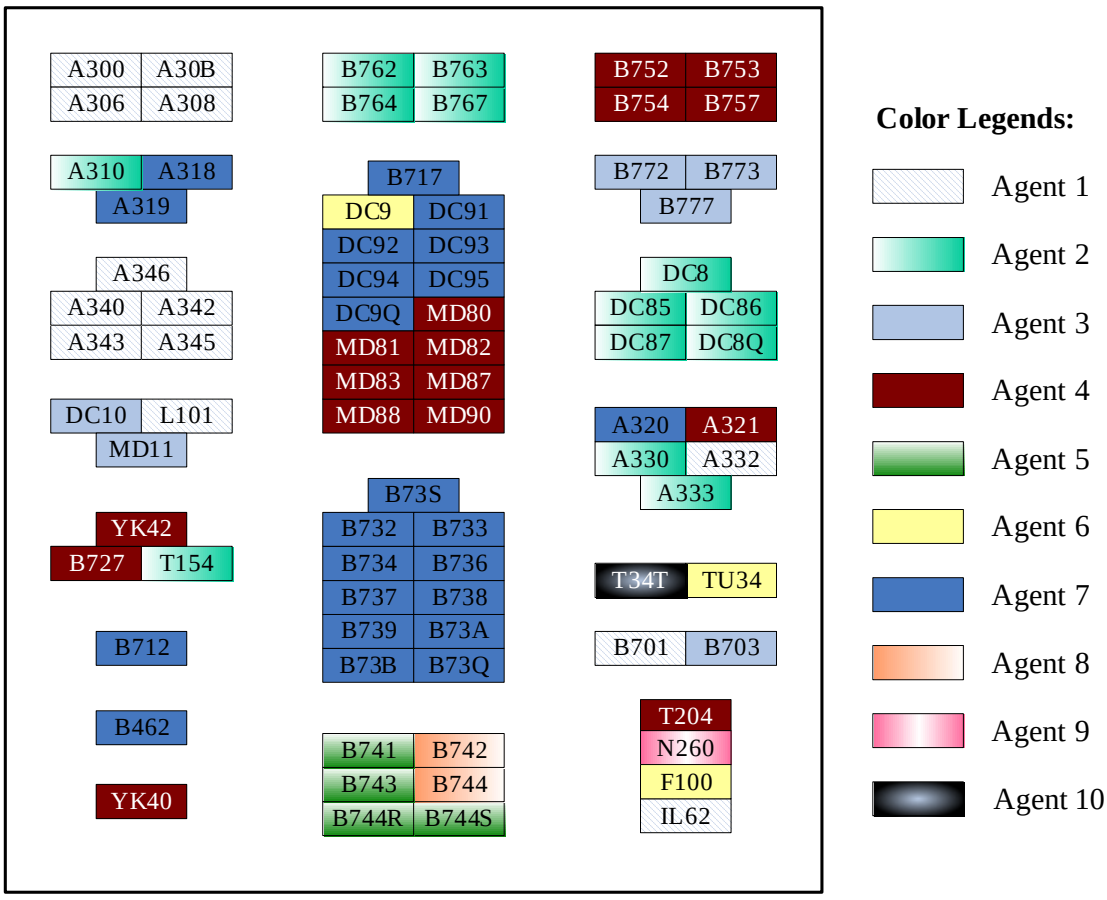

Figure 4-10: The mapping of multi-agent collectives: the spatial mapping refers to the results of manual aggregation, the color mapping refers to the results of the developed algorithm.

Some aircraft types that are clustered together in Figure 4-10 are also assigned the same color. There are 16, out of 19, agents formed by the manual aggregation that have more than one aircraft type as members. Seven of those agents are also formed by the surrogate modeling method. This observation shows that the developed surrogate modeling method is indeed able to group together aircraft types that are, by engineering judgment, similar.

2. Separation by the surrogate modeling method of aircraft types that are considered similar by engineering judgment.

   Figure 4-11 shows a sample case where aircraft types that are grouped together by the manual aggregation method are separated by the developed surrogate modeling method.

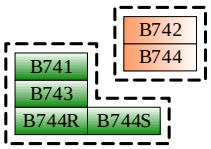

Figure 4-11: A sample case where an agent that is formed by the manual aggregation method is separated by the surrogate modeling method.

Two aircraft types are selected for further analysis: the Boeing B742 and B74S. Their linear approximations for fuel burn estimation are shown in Table 4.5. The difference in the computed gradients is also shown in Figure 4-12, with the corresponding gradient ratios are -21.59% when the test aircraft type is B742 and 27.53% when the test aircraft type is B74S.

B742	$f_{i\,B742} \approx 0.0136 \cdot d_{i\,B742}$
B74S	$f_{i\,B74S} \approx 0.0107 \cdot d_{i\,B74S}$

Table 4.5: Linear approximations for fuel burn estimation for the B742 and B74S.

3. Recognition of some *latent identities* by the surrogate modeling method.

   In this context, the latent identities refer to similar aircraft type characteristics that are not easily observable by engineering judgment alone. These latent identities are observed in Figure 4-10 in aircraft types that are not clustered together, but are assigned the same color. It is also observed that there are two cases where two agents

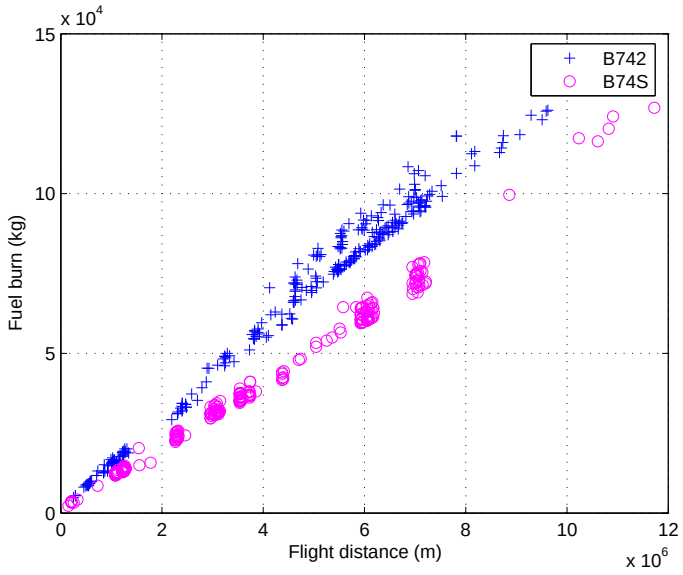

Figure 4-12: The fuel burn vs distance plots of two aircraft types (B742 and B74S) that are considered similar by engineering judgment but are separated into two agents by the developed surrogate modeling method.

that are formed by manual aggregation are joined together by the surrogate modeling method (refer to Figure 4-13).

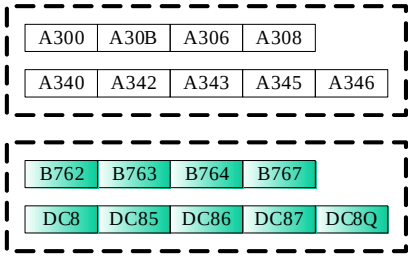

Figure 4-13: Two sample cases where agents that are formed through the manual aggregation are joined together by the surrogate modeling method. In this figure, the rows of aircraft types are agents formed by the manual aggregation method. When they are joined together by the surrogate modeling method, they are clustered in the same box.

For further analysis, we select two aircraft types that are different by their physical characteristics, but exhibit a similar relationship between the fuel burn and flight distance. The two aircraft types are the Douglas DC10 and Boeing B777. Their linear approximations for fuel burn estimation, which are given in Table 4.6, show similar gradients. The computed gradient ratios corresponding to these two gradients are

1.27% when the test aircraft type is B777 and -1.25% when the test aircraft type is DC10. The similarity between the gradients can also be seen in Figure 4-14, where cruise fuel burn is plotted against cruise distance for the two aircraft types. A comparison between the physical characteristics of these two aircraft types is tabulated in Table 4.7. The two aircraft types are not grouped together in the manual aggregation mainly due to the different number of engines, and also the age of the aircraft. The DC10 was first launched in 1968, which was much earlier than the first launch of the B777 in 1990. Thus, the engine of the DC10 is assumed to be less efficient than the newer generation engine of the B777. Further, the DC10 has three engines, whereas the B777 is operated with only two engines. There might be a tradeoff between these factors, i.e., the age and number of engines as well as the difference in range capacities, that is recognized by the surrogate modeling method.

DC10	$f_{i\,DC10} \approx 0.0088 \cdot d_{i\,DC10}$
B777	$f_{i\,B777} \approx 0.0089 \cdot d_{i\,B777}$

Table 4.6: Linear approximations for fuel burn estimation for the DC10 and B777.

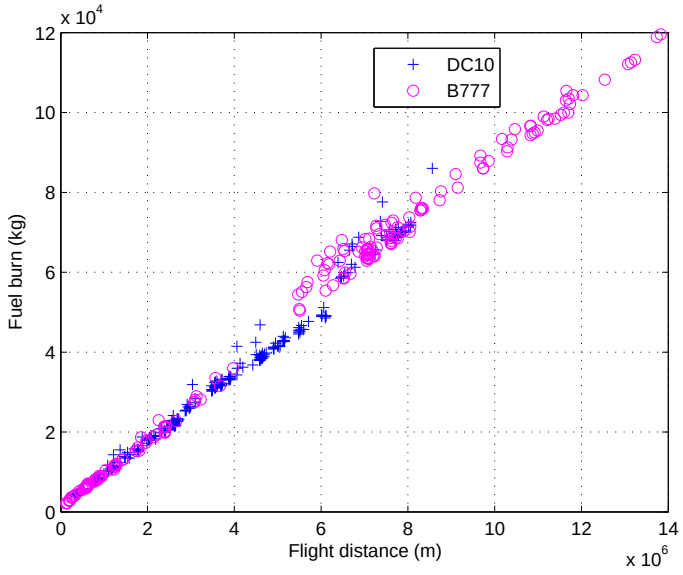

Figure 4-14: The fuel burn vs distance plots of two aircraft types (DC10 and B777) that are not grouped together by the manual aggregation method but are joined together by the surrogate modeling method.

Aircraft Type	Boeing B777	Douglas DC10
Category	Long-range high capacity widebody airliner	Medium to long-range widebody airliner
Year of origin	1990	1968
No. of engine	2	3
Wing span	60.93 m	50.41 m
Length overall	63.73 m	55.50 m
Height overall	18.51 m	17.70 m
Wing area	427.8 m^2	367.7 m^2
Operating weight empty	141,340 kg	121,198 kg
Max take-off weight	247,210 kg	263,085 kg
Max landing weight	210,850 kg	182,978 kg
Max payload	29,050 kg	48,330 kg
Max cruising speed	923 km/h	982 km/h
Passenger capacity	375-400	up to 380

Table 4.7: Specification comparison for the Douglas DC10 and Boeing B777 [14].

Compared to the result from the manual aggregation, the surrogate modeling method is able to provide better results, which is evident in both the total number of agents created and the computed total estimation errors. The maximum number of agents created by the surrogate modeling method is 17, when the threshold value is set to 10%, as shown in Figure 4-6. Figure 4-6 also shows that the method is able to achieve a maximum absolute value of the total estimation errors of just 2.08% with ten agents. This maximum error value is lower than the error obtained from manual aggregation, i.e., 3.25%.

Although in this case manual aggregation is able to provide a surrogate model with acceptable total estimation error, the systematic approach identifies latent identities that are not apparent to simple engineering judgment and separates identities that are considered similar by engineering judgment, which lead to a more effective surrogate model. Further, the manual approach relies on subjective decisions that may vary from person to person, while the proposed method utilizes an objective metric to identify groupings. Finally, as the number of units increases, the complexity of the aggregation task becomes much greater, and may be overwhelming to perform manually.

Chapter 5

Surrogate Modeling for Emissions Estimation

This chapter presents the demonstration of the developed surrogate modeling method, applied to the emissions estimation model within APMT. The emissions species CO_2, H_2O, SO_x, CO, HC, and NO_x are considered in this case study. This chapter begins by explaining the formation of the surrogate model. The surrogate model derived by the developed surrogate modeling method is then presented and discussed.

5.1 Multi-Agent Collective Formation

The first step in implementing the surrogate modeling method is to select the appropriate aggregation unit. To make the selection for this specific case study, the emissions computations performed in SAGE are considered. Based on the computations described in Chapter 2, emissions species can be classified into two groups. In the first group of species, comprising CO_2, H_2O, and SO_x, the emissions are computed as scalar multiplications of fuel burn values. The emissions computations for the species included in the second group (CO, HC, and NO_x), on the other hand, employ a curve-fitting method, i.e., the Boeing Fuel Flow Method 2 (BFFM2). The curve, obtained from the ICAO emissions databank, is unique for each engine type. Figure 5-1 displays plots of emissions against flight distance for the T154 aircraft type, which is arbitrarily selected for display purposes. The plots distinguish the two engine types associated with the T154. The figure shows that for flights that belong to the same aircraft type, the emissions computations for the first group of species are

independent of the engine type, whereas the computations for the second group of species shows the dependence on the engine type.

Two important aspects of the surrogate modeling procedure are established based on the observations made from Figure 5-1:

1. Selection of the aggregation unit.

   Figure 5-1 shows that an aircraft/engine (AE) pair has a distinct relationship between emissions (particularly for CO, HC, and NO_x) and flight distance, compared to other pairs. Based on this observation, an AE pair is selected to be the aggregation unit for the second case study. This selection of aggregation unit is applicable to all emissions species, despite the different emissions computations.

   In this research, we consider 259 AE pairs that correspond to the 82 aircraft types used in the previous case study. To reduce the computational cost for querying the data for these 259 AE pairs, only data from the months of January, July, and December in SAGE Flight Inventory for 2005 (Ξ_{2005}) are used in this analysis. The term *total emissions* mentioned in this discussion specifically refers to the summation of all emissions estimates that belong to the aforementioned months. As in the previous case study, only the cruise segment of flight is considered in this analysis.

2. Collective computational task.

   A linear functional approximation, as used in the previous case study, is also implemented to compute the emissions estimates for each AE pair. Figure 5-1 shows that the relationship between emissions and flight distance is approximately linear for a particular AE pair.

The surrogate modeling procedure that is used in Chapter 4 can be leveraged for this case study. This procedure, tailored for the surrogate modeling for emissions estimation, is summarized in Table 5.1.

The computations required to carry out the surrogate modeling method are derived in a similar manner to the corresponding equations in Chapter 4. To rate the performance of agents, the total estimation error, ε, is also used for this case study. These equations are listed in Table 5.2, where the total emissions is denoted by $\mathbf{E}$ and the total number of AE pairs is denoted by N_{AE}, to replace $\mathbf{f}$ and N_{AC} that are used in the previous chapter. Note

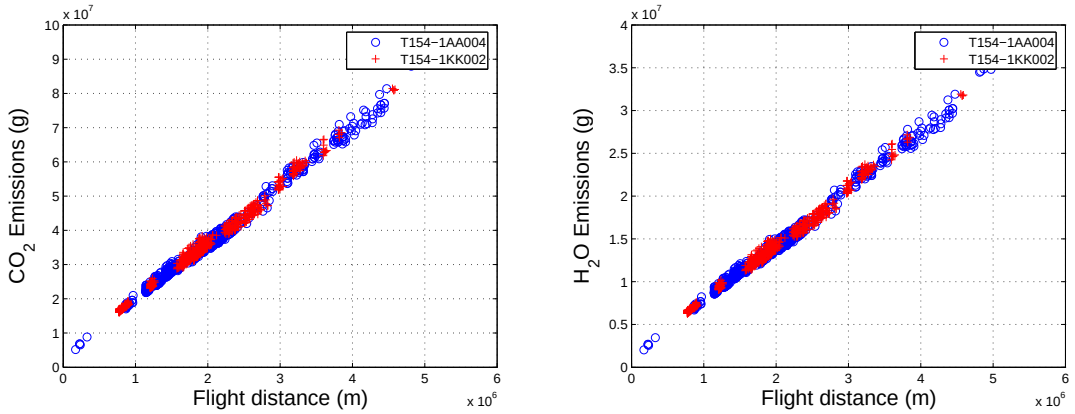

(a) CO_2 emissions

(b) H_2O emissions

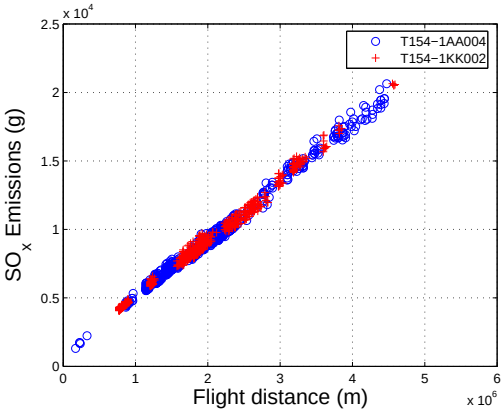

(c) SO_x emissions

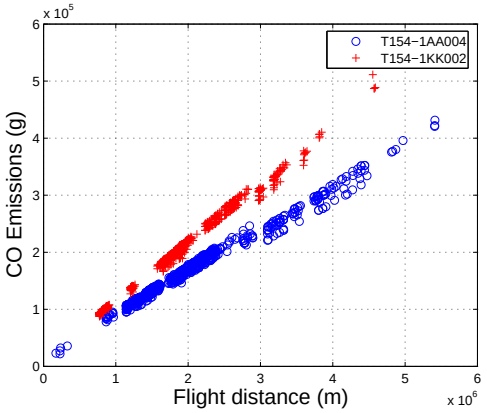

(d) CO emissions

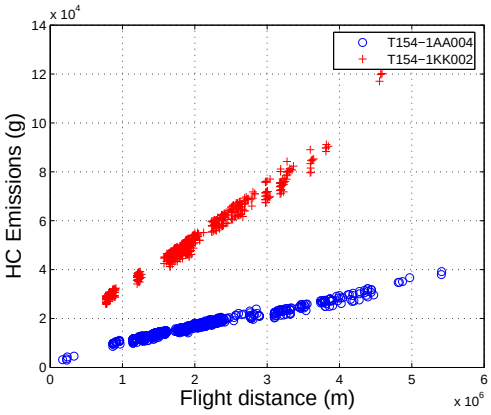

(e) HC emissions

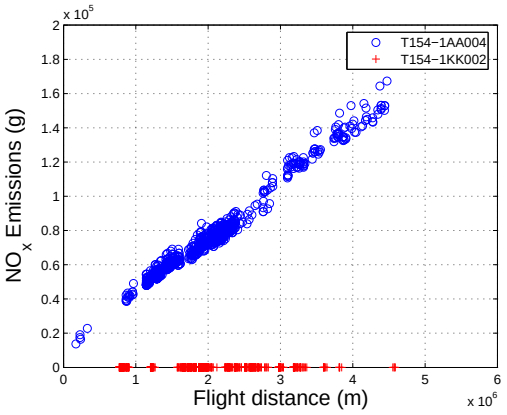

(f) NO_x emissions

Figure 5-1: Plot of cruise emissions against cruise distance for the T154 aircraft type with two engine types: 1AA004 and 1KK002.

Surrogate Modeling Component	**Specification for emissions estimation example**
Aggregation unit	Aircraft/Engine (AE) pair.
Emissions computation for each unit	A functional approximation by a linear regression analysis performed on cruise emissions and cruise distance.
Aggregation criteria	Cross-estimation error, ε_c, and a threshold value, δ_t.
Similarity assessments	Evaluation of cross-estimation errors between any two units. The gradient ratio, γ (Equation 4.15), is used as the *a priori* cross-estimation error approximation.
Aggregation procedure	Formation of primary and coarse agents. The procedure is similar to the algorithm illustrated in Figure 4-3, but replacing aircraft type by AE pair. Finalization (refinements) of agents. The procedure follows the algorithm illustrated in Figure 4-4.
Selection of the agent representative	An AE pair that travels the maximum total distance within an agent is selected to be the agent representative.

Table 5.1: Summary of the surrogate modeling procedure for emissions estimation, which is leveraged from the fuel burn estimation case study presented in Chapter 4.

that, in the table, the variable **E** is used generically for all emissions species. The notations used in the equations are also changed accordingly from Chapter 4; i denotes the index of a flight within an AE pair, j denotes the index of an AE pair in a data set, $N_{f\,j}$ refers to the total number of flights within the j-th AE pair, and A_k refers to the set of AE pairs included in the k-th agent.

Description	**Equation**
Total emissions per AE pair	$\mathbf{E}_j = b_{1\,j} \cdot \sum_{i=1}^{N_{f\,j}} d_{i\,j} + N_{f\,j} \cdot b_{0\,j}$
Total emissions estimates per agent	$\tilde{\mathbf{E}}_{a\,k} = b_{1\,k} \cdot \sum_{j \in A_k} \sum_{i=1}^{N_{f\,j}} d_{i\,j} + b_{0\,k} \cdot \sum_{j \in A_k} N_{f\,j}$
Cross-estimation error	$\varepsilon_c = \dfrac{\tilde{\mathbf{E}}_t - \mathbf{E}_t}{\mathbf{E}_t} \cdot 100\%$
Individual agent's estimation error	$\varepsilon_k = \dfrac{\tilde{\mathbf{E}}_{a\,k} - \sum_{j \in A_k} \mathbf{E}_j}{\sum_{j \in A_k} \mathbf{E}_j} \cdot 100\%$
Total estimation error	$\varepsilon = \dfrac{\sum_{k=1}^{N_{agent}} \tilde{\mathbf{E}}_{a\,k} - \sum_{j=1}^{N_{AE}} \mathbf{E}_j}{\sum_{j=1}^{N_{AE}} \mathbf{E}_j} \cdot 100\%$

Table 5.2: The equations used in the surrogate modeling for emissions estimation that are leveraged from the fuel burn estimation aggregation. The derivations of these equations are presented in Chapter 4, in the context of computing fuel burn estimates.

5.2 Results

This section first presents the surrogate model derived based on Ξ_{2005} for emissions estimation and the computed estimation errors. A study of the individual agents' estimation

errors is then discussed, by focusing on the surrogate model derived for NO_x emissions estimation. Next, we further investigate error trends exhibited by the results, their possible causes, and their implications for the formation of a multi-agent collective.

5.2.1 The Surrogate Model

The total emissions estimated using the derived surrogate model, for CO_2, H_2O, SO_x, CO, HC, NO_x, are studied by varying the threshold value, δ_t. In this analysis, the threshold values are varied between 10% and 25%, with 1% increment. As emissions estimates for CO_2, H_2O, and SO_x are a scalar multiplication of each other, the corresponding number of agents created and total estimation errors of those species are identical, and are shown in Figure 5-2. The plots for CO, HC, and NO_x emissions are given in Figures 5-3, 5-4, and 5-5, respectively.

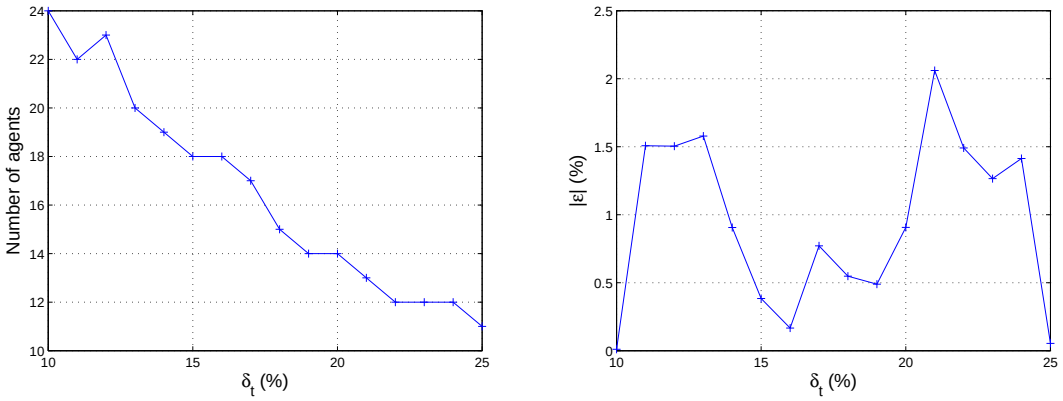

(a) Variation of number of agents

(b) Variation of $|\varepsilon_e|$

Figure 5-2: Aggregation results for CO_2, H_2O, and SO_x emissions computation with varying threshold values.

From Figures 5-2 to 5-5, we observe that the total number of agents formed from the surrogate modeling procedure tends to decrease with increasing threshold value. The total estimation errors, on the other hand, do not exhibit any observable trends. As in the previous case study, individual agents' estimation errors are analyzed. In this thesis, only plots pertaining to the surrogate model derived based on NO_x emissions data are presented. The analyses include comparing the maximum absolute values of individual agents' estimation errors and the corresponding total estimation errors (Figure 5-6); and observing the distribution of individual agents' estimation errors. For the latter analysis, the error distributions

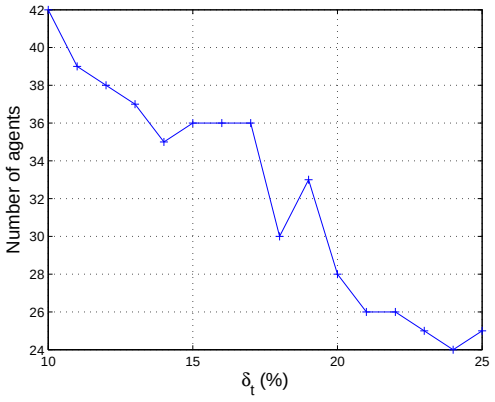

(a) Variation of number of agents

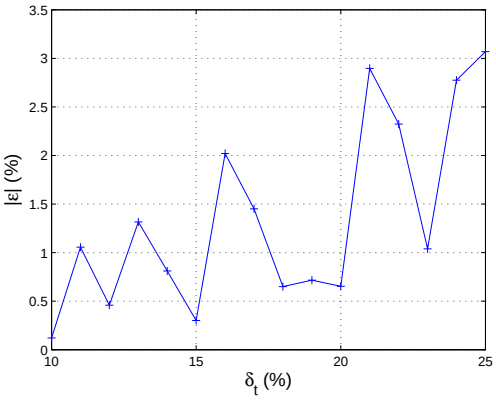

(b) Variation of $|\varepsilon_e|$

Figure 5-3: Aggregation results for CO emissions computation with varying threshold values.

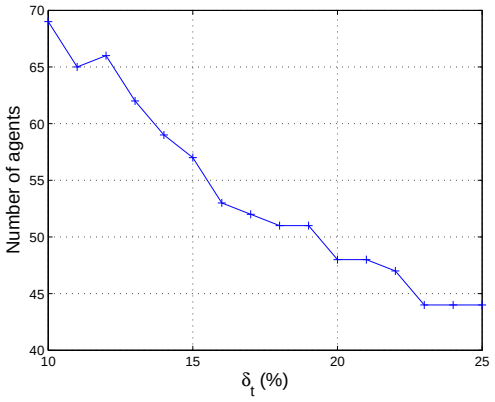

(a) Variation of number of agents

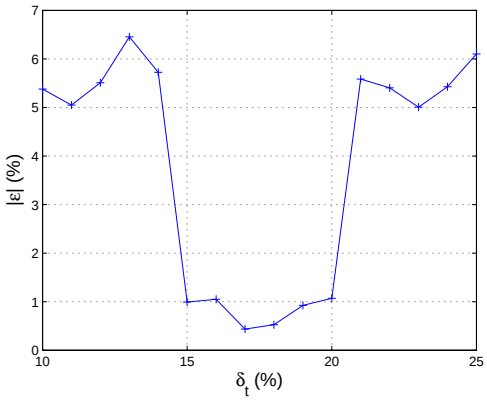

(b) Variation of $|\varepsilon_e|$

Figure 5-4: Aggregation results for HC emissions computation with varying threshold values.

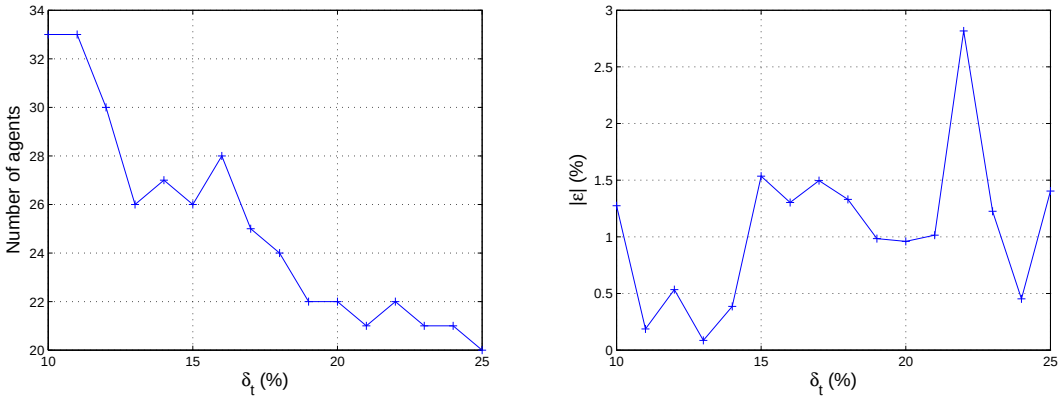

(a) Variation of number of agents

(b) Variation of $|\varepsilon_e|$

Figure 5-5: Aggregation results for NO_x emissions computation with varying threshold values.

corresponding to four threshold values are displayed in Figure 5-7. The mean and standard deviation, σ, of the distribution of individual agents' estimation errors are also shown in each plot.

Figures 5-6 and 5-7 show similarities with the previous analyses in the first case study, as discussed in Chapter 4. Some observations from the figures are:

1. The computed maximum individual agent's estimation error is 16.84%, which is observed when a threshold value of 22% is used. This threshold value corresponds to the maximum total estimation error in the analysis.

2. Surrogate models that have a large total estimation error tend to have a large standard deviation in the distribution of individual agents' estimation errors. This is not the case, however, with a threshold value of 15%. The computed total estimation error with this threshold value is higher than when computed with a threshold value of 13%, although the standard deviation of the former is smaller than the latter. The higher computed mean at the former accounts for this occurence.

3. The computed total estimation error is always lower than the maximum absolute individual agent's estimation error at a given threshold value, as displayed in Figure 5-6.

Figures 5-8 and 5-9 show the multi-agent collective formed when a threshold value of 15% is used in the surrogate modeling for NO_x emissions estimation, with a total estimation

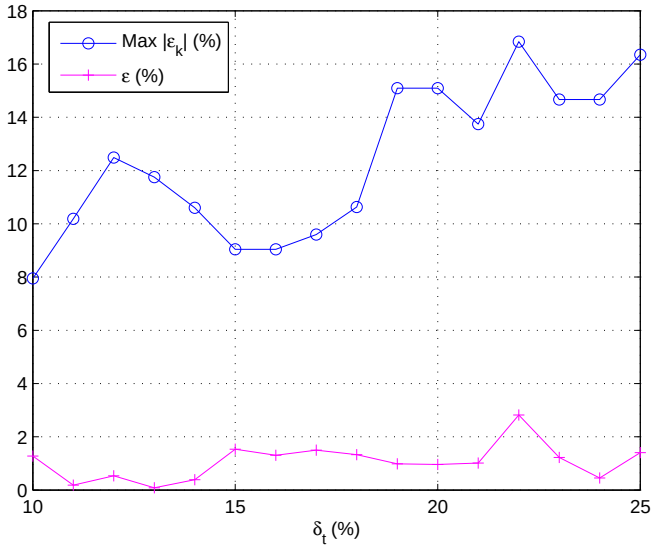

Figure 5-6: Comparison between the computed total estimation errors and the maximum absolute values of individual agents' estimation errors at various threshold values.

error of 1.54%. In the figures, the formed agents are identified by the clustering of the AE pairs. The colors differentiate engine manufacturers of the AE pairs. The multi-agent collectives for other species, also when a threshold of 15% is used, are given in Appendices B to D. These results show that for CO, HC, and NO_x emissions estimations, an AE pair is a more effective aggregation unit than an aircraft type, as used in the previous case study. The agents formed for CO, HC, and NO_x emissions estimations do not group all AE pairs that belong to the same aircraft type together. This observation consolidates our earlier argument that the emissions computations for these species also depend on the engine type. The aggregation result presented in Appendix D, on the other hand, shows that the multi-agent collective formed for CO_2, H_2O, and SO_x emissions estimations group most AE pairs that belong to the same aircraft type together.

In Figure 5-1, relationships between emissions and flight distance are observed for different engine types within T154, i.e., 1AA004 and 1KK002. In the multi-agent collectives formed for CO, HC, and NO_x, T154-1AA004 and T154-1KK002, marked with red boxes, belong to different agents. For this group of emissions species, the two engine types exhibit distinct trends when the emissions are plotted against the flight distance in Figure 5-1. For other species, nonetheless, T154-1AA004 and T154-1KK002 belong to the same agent,

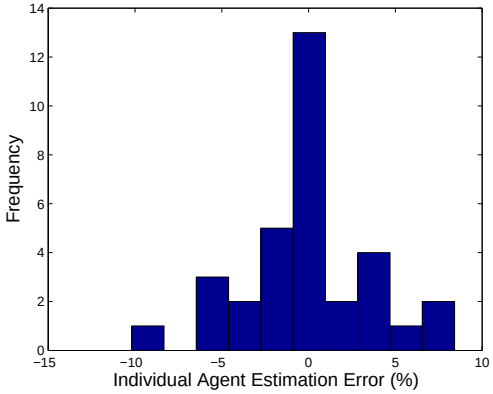

(a) Minimum error #1, threshold = 11%. Mean = -0.13%, σ = 3.75%.

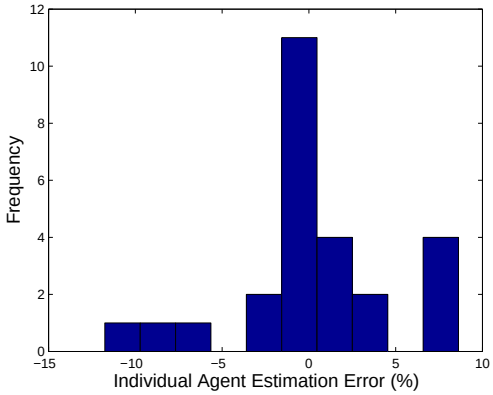

(b) Minimum error #2, threshold = 13%. Mean = 0.32%, σ = 4.70%.

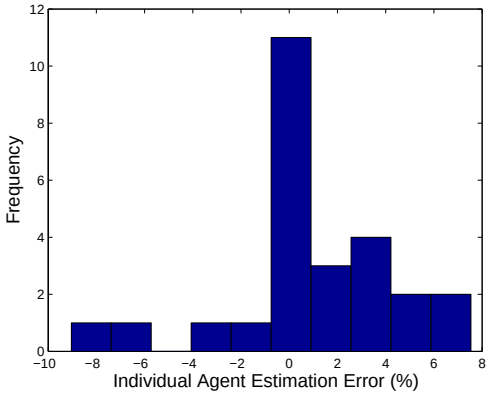

(c) Maximum error #1, threshold = 15%. Mean = 0.88%, σ = 3.64%.

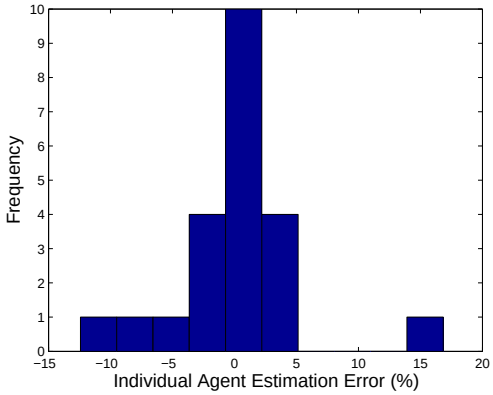

(d) Maximum error #2, threshold = 22%. Mean = -0.12%, σ = 5.50%.

Figure 5-7: Four distributions of individual agents' estimation errors for NO_x emissions computation: two threshold values have maximum total estimation errors, and the other two have minimum total estimation errors.

which is consistent with the similar trends exhibited in their emissions against flight distance plots.

5.2.2 Discussion

To compare the results for emissions and fuel burn estimations, the multi-agent collective formation for fuel burn estimation is run using flight data from January, July, and December in Ξ_{2005}; thus, the results presented below are obtained using the same data set. Compared to the results for the fuel burn estimation case study, higher total estimation errors are observed in the computations for CO, HC, and NO_x emissions. The minimum and maximum total estimation errors for fuel burn and emissions estimations, for all species, are presented in Table 5.3.

Description	Minimum $\|\varepsilon\|$	Maximum $\|\varepsilon\|$
Fuel burn	0.01%	2.65%
CO_2, H_2O, SO_x emissions	0.01%	2.06%
CO emissions	0.12%	3.07%
HC emissions	0.44%	6.50%
NO_x emissions	0.09%	2.87%

Table 5.3: Minimum and maximum total estimation errors in fuel burn and emissions estimations.

Table 5.3 shows that the minimum total estimation error for CO_2, H_2O, SO_x emissions is the same, up to two decimal points, to the total estimation error for fuel burn estimation. The maximum total estimation error for this group of emissions species is, however, lower than the maximum total estimation error computed for the fuel burn estimation. Note that the computations for CO_2, H_2O, SO_x emissions are just scalar multiplications of the fuel burn computation. Thus, their collective computational tasks are considered similar. Different selection of the aggregation unit for the two tasks is believed to explain these observations of the computed errors. The aggregation unit selected for the CO_2, H_2O, SO_x emissions estimations (AE pair) is more refined than the aggregation unit used in the fuel burn estimation (aircraft type), which allows for a finer formation of agents. At the beginning of this chapter, it was mentioned that the CO_2, H_2O, SO_x emissions computations for flights that belong to the same aircraft type are, in general, independent of the engine type. Nonetheless, slight differences may exist. Thus, using an AE pair instead of an aircraft

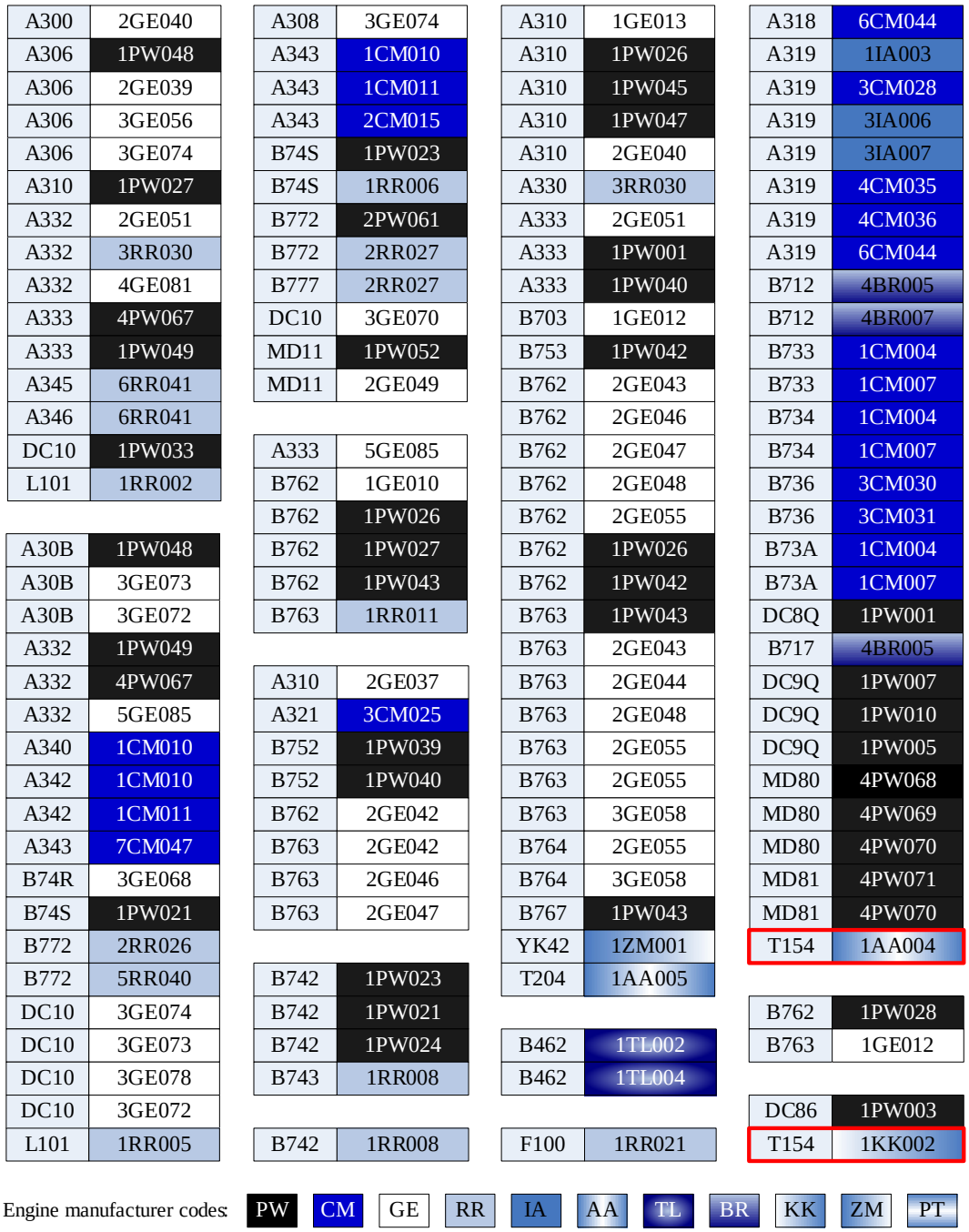

Figure 5-8: Part 1: Agents formed for NO_x emissions aggregation, with threshold value 15%, and the total estimation error 1.54%. The formed agents are identified by the spatial clusterings of AE pairs, and the colors differentiate the engine manufacturers.

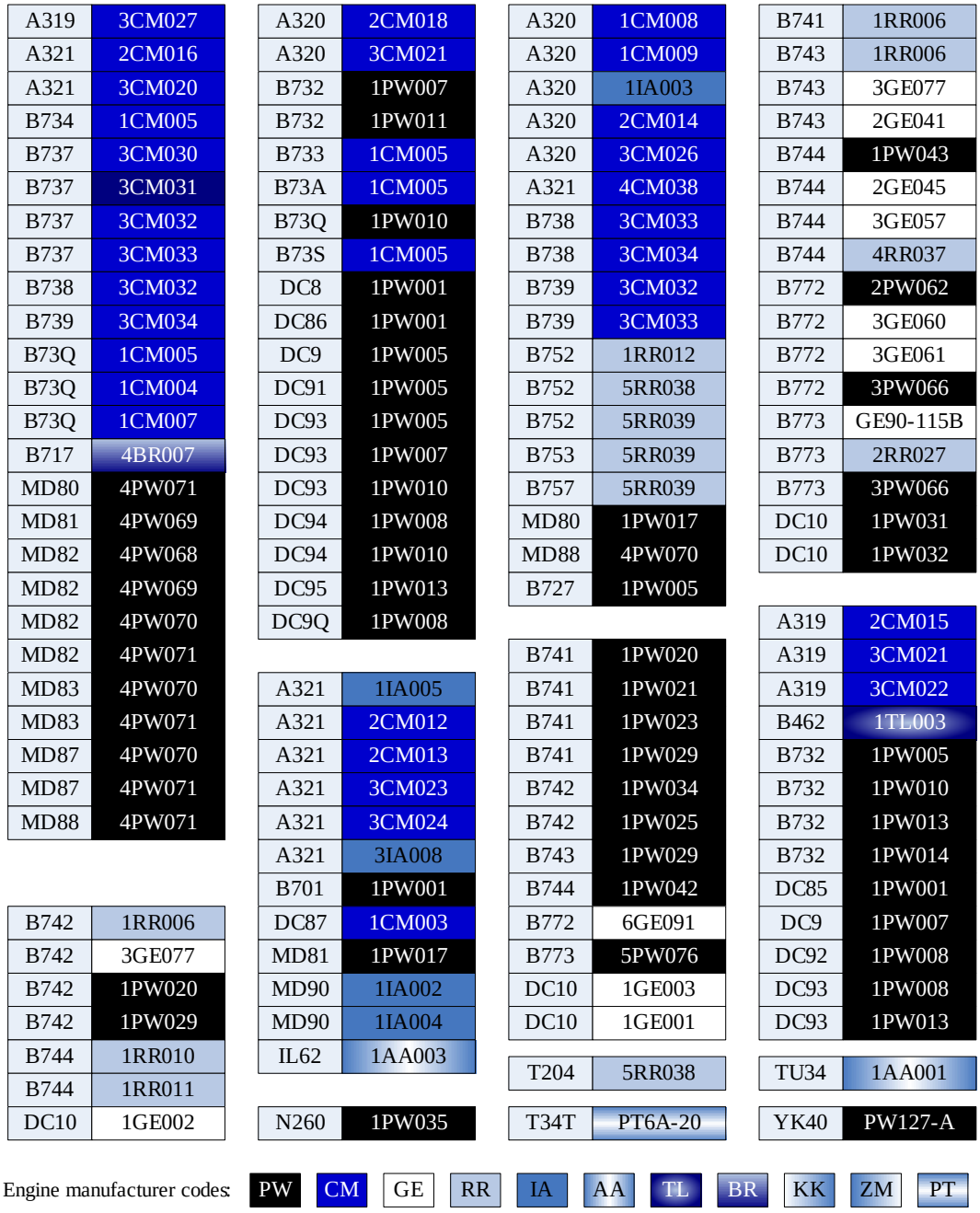

Figure 5-9: Part 2: Agents formed for NO_x emissions aggregation, with threshold value 15%, and the total estimation error 1.54%. The formed agents are identified by the spatial clusterings of AE pairs, and the colors differentiate the engine manufacturers.

type as the aggregation unit can result in a better surrogate model for the same collective computational task.

The maximum total estimation error is observed for the estimation of HC emissions. Figure 5-4 (b) shows that there is a sharp decrease of total estimation error when a threshold value of 15% is used. We further investigate this result by comparing the surrogate models obtained when threshold values of 13%, which yields a total estimation error of 6.46%, and 16%, which yields a total estimation error of 1.05%, are used. A very high individual agent's estimation error is observed when a threshold value of 13% is used, i.e., 57.56%. This individual agent's estimation error propagates through to the high total estimation error. The AE pairs that belong to this particular agent are listed in Table 5.4, with the agent representative typed in bold. The table also shows the regression parameters, $b_{1\,j}$ and $b_{0\,j}$, for each AE pair.

AE pair	$b_{1\,j}$	$b_{0\,j}$
B741-1PW020	0.0035	13,400.00
A310-1GE013	0.0034	699.84
B741-1PW029	0.0032	280.84
B742-3GE077	0.0035	1,033.30
B742-1PW020	0.0035	11,769.00
B742-1PW021	0.0034	11,553.00
B742-1PW029	0.0035	981.67
B743-3GE070	0.0031	679.43
B743-1PW029	0.0032	20.65
B74R-3GE068	0.0030	709.76
B762-1GE010	0.0032	858.71
B762-1GE012	0.0033	1,225.40
B763-1GE012	0.0033	997.14
B763-1RR011	0.0033	-173.64
DC92-1PW008	0.0030	555.69
DC93-1PW008	0.0029	676.21
DC94-1PW008	0.0030	690.87
DC9Q-1PW008	0.0030	597.55
DC10-1PW031	0.0033	12,080.00
DC10-1PW033	0.0032	2,843.70

Table 5.4: An agent formed in HC emissions estimation when a threshold value of 13% is used, with a corresponding individual agent's estimation error of 57.56%.

Although the gradients of linear regression equations for AE pairs listed in Table 5.4 are close to each other, the constant terms ($b_{0\,j}$) vary greatly. The selected agent representative

is the B741-1PW020, and the constant term corresponding to its linear equation is 13,400. The linear equation of this representative AE pair is used to estimate the total HC emissions of the agent. The large value of $b_{0\,j}$ in the equation will overestimate the emissions computation of the agent considerably, as it will be multiplied by the total number of flights included in the agent (refer to the equation in Table 5.2). A similar agent is formed when a threshold value of 16% is used. The B741-1PW020 is, however, excluded from the agent; instead, it forms another agent with the B741-1PW021. With the B741-1PW020 removed from the agent, the computed individual agent's estimation error is -5.72%, which is much lower in magnitude than the earlier computed error of 57.56%. The representative AE pair for this new agent is the B762-1GE010. The agent that comprises B741-1PW020 and B741-1PW021 yields an individual agent's estimation error of -0.57%. These lower individual agents' estimation errors account for the lower total emissions error at the aggregated level. This observation is discussed further in the following.

A higher threshold value may allow more units to be grouped together into an agent at the initial stage of agent formation. Subsequent assessments in the aggregation procedure, however, may separate the agent to obtain a better surrogate model. In the sample case presented above, a threshold value of 16% initially included B741-1PW021 in the agent tabulated in Table 5.4. During the refinement of agents (Step 3 in Figure 3-4), B741-1PW020 and B741-1PW021 are separated from the former agent, which leads to the formation of a better surrogate model. From the above discussion, we conclude that:

1. Although the gradient ratio works well as the *a priori* estimation error approximation in the fuel burn estimation case study, it is found to be insufficient for this case study. Further improvement can be made by considering the constant term in the linear regression equation corresponding to each unit to derive a better *a priori* estimation error approximation.

2. There is no a direct relationship between the threshold value and the total estimation error. At the early stage of the aggregation procedure, the agent formation may be less stringent when a higher threshold value is used. Subsequent assessments in the procedure, however, may refine these agents to form a better surrogate model than when a smaller threshold value is used.

3. Table 5.3 shows that small total estimation errors, e.g., below 2%, are attainable in the

emissions estimation for all species. Future research may devise a systematic method to find the threshold value that corresponds to the minimum total estimation error, by also considering the number of agents formed by the procedure.

Chapter 6

Conclusions and Recommendations

6.1 Summary and Conclusions

Existing surrogate modeling methods have limited applicability to large-scale black-box systems with many inputs. This research aims to devise a systematic method to enable complexity reductions for this class of systems by reducing the dimension of the input space. The systems of interest in this research are constructed by a number of independent units. The surrogate model is created by aggregating similar units together into agents; the collection of these agents forms a *multi-agent collective*. The representatives selected from the formed agents will, collectively, perform an inexpensive computation in place of the complex computational task that the full system needs to complete. There are three key steps in the formation of a multi-agent collective: a proper selection of the aggregation unit, which is largely dependent of the computational task at hand; the aggregation procedure to form agents, which relies on the *similarity assessments* between units; and the selection of a representative unit from each agent.

The surrogate modeling method is demonstrated on two case studies in the context of the fuel burn and emissions estimation model within the Aviation Environmental Portfolio Management Tool (APMT). The first case study considers a flight inventory comprising 82 aircraft types, as the aggregation units, to compute fuel burn estimates. The second case study focuses on computing emissions estimates, including CO_2, H_2O, SO_x, CO, HC, and NO_x emissions species. In the latter case study, an aircraft/engine (AE) pair is selected to be the aggregation unit. There are 259 AE pairs considered in this case. The similarity assessments between units are done by comparing each unit's relationship

between fuel burn, for the first case study, or emissions, for the second case study, and the flight distance, which is approximately linear. The gradients of the linear functional approximations that are derived from the available flight information are used to assess the similarity between two units, by computing the *gradient ratio* of the two units. A threshold value is defined to adjust the stringency of the aggregation procedure. The effectiveness of a surrogate model is evaluated by measuring the total estimation error, that is, the discrepancy between outputs—total fuel burn or emissions estimates—from the full and surrogate models.

Ten aircraft types are selected by the surrogate modeling procedure to compute fuel burn estimates, yielding a total estimation error of just 2.08%, which is deemed acceptable based on previous studies in the field. Similar results are observed in the CO_2, H_2O, and SO_x emissions estimations, which are just scalar multiplications of fuel burn. The analyses carried out for the CO, HC, and NO_x emissions estimation show that the number of formed agents tends to decrease with increasing threshold values. The total estimation errors, on the other hand, do not exhibit any distinct relationships with the threshold values. An investigation into this lack of trends suggests that although the threshold value controls the formation of agents at the initial stage of the aggregation procedure, further refinements of agents may result in a better surrogate model than when a more stringent threshold value is used. In addition, the effects of stringency of the agent formation become smaller when propagated through to an aggregated level, as concluded by studying the distribution of individual agents' estimation errors and the corresponding total estimation error. We discover that some agents contain AE pairs with similar gradients in the linear equations relating emissions and flight distance but with a large difference in the constant terms. Surrogate models with such agents have larger total estimation errors than others.

The maximum total estimation error computed from applying the surrogate model derived for fuel burn estimation to other flight inventory data sets is 2.1%, which is deemed acceptable. This finding suggests that the surrogate model can be derived once in an *offline stage*, and used to perform the computational tasks on different data sets repeatedly in an *online stage*, while maintaining the accuracy. The surrogate model for the fuel burn estimation is also compared to another model that aggregates aircraft types based on engineering judgment—the manual aggregation method. The systematic method yields fewer agents and a lower total estimation error. In addition, the systematic approach is more reliable

than manual aggregation, especially for systems with a large number of units, as it does not rely on subjective decisions, which can vary from person to person.

6.2 Future Recommendations

There are a few improvements for the developed surrogate modeling method to obtain more effective and accurate surrogates for the two case studies considered in this research, based on the earlier discussions of the results. Firstly, we need to have a better similarity assessment method between units. We may consider other factors, such as the constant term in the linear functional approximations used in the analyses and the range of distance traveled by flights within an aircraft type or AE pair, to derive a more effective measure to quantify the similarity between units. As discussed previously, total estimation errors vary with threshold values, with no distinct trends. A search procedure can be introduced in the method to find the optimum threshold value, taking the number of agents and total estimation error into consideration.

It is desirable to be able to control the effectiveness of surrogate models by adjusting parameters used in the surrogate modeling procedure. Due to the lack of governing equations in black-box systems, derivation of an *a priori* error estimation at the aggregated level is a significant challenge, if not impossible. A different approach might be to derive a metric that provides an upper bound of the estimation error at the agent level; one possible metric is the threshold value. A challenge remains in studying the relationship between the aggregation criteria, in particular the threshold value, and an individual agent's estimation error to ensure the validity of the upper bound in all cases.

It is clear that accurate approximations of large-scale black-box systems by surrogate models are crucial to enable expensive analyses, which would otherwise be computationally prohibitive. One such analysis is a Monte Carlo simulation, which typically requires thousands of simulations to be run. For this purpose, we must ensure that the surrogate models are able to capture the characteristics and the associated uncertainties of the full models accurately.

Appendix A

List of Aircraft Types

Aircraft Code	Aircraft Name
A300	Airbus A300
A30B	Airbus A300B4-200
A306	Airbus A300B4-600
A308	Airbus A308
A310	Airbus A310
A318	Airbus A318
A319	Airbus A319
A320	Airbus A320
A321	Airbus A321
A330	Airbus A300
A332	Airbus A300-200
A333	Airbus A300-300
A340	Airbus A340
A342	Airbus A340-200
A343	Airbus A340-300
A345	Airbus A340-500
A346	Airbus A340-600
B462	BAE 146-200/RJ
B701	Boeing 707-100

continued on the next page

continued

A/C Code	Aircraft Name
B703	Boeing 707-300
B712	Boeing 717-200
B717	Boeing 717
B727	Boeing 727
B732	Boeing 737-228
B733	Boeing 737-300
B734	Boeing 737-400
B736	Boeing 737-600
B737	Boeing 737-700
B738	Boeing 737-800
B739	Boeing 737-900
B73A	Boeing 737-100/200
B73B	Boeing 737-300/400/500
B73Q	Boeing 737 Stage 3
B73S	Boeing 737-SP
B741	Boeing 747-100
B742	Boeing 747-200
B743	Boeing 747-300
B744	Boeing 747-400
B74R	Boeing 747-SR
B74S	Boeing 747-SP
B752	Boeing 757-200
B753	Boeing 757-300
B754	Boeing 754
B757	Boeing 757
B762	Boeing 767-200
B763	Boeing 767-300
B764	Boeing 767-400
B767	Boeing 767-200ER/300/300ER

continued on the next page

continued

A/C Code	Aircraft Name
B772	Boeing 777-200
B773	Boeing 777-300
B777	Boeing 777
DC10	Douglas DC10
DC8	Douglas DC-8
DC85	Douglas DC-85
DC86	Douglas DC-86
DC87	Douglas DC-87
DC8Q	Douglas DC-8 Stage 3
DC9	Douglas DC-9
DC91	Douglas DC-9 /10
DC92	Douglas DC-9 /20
DC93	Douglas DC-9 /30
DC94	Douglas DC-9 /40
DC95	Douglas DC-9 /50
DC9Q	Douglas DC-9 Stage 3
MD11	McDonnell-Douglas MD-11
MD80	McDonnell-Douglas MD-80
MD81	McDonnell-Douglas MD-80/ 81/
MD82	McDonnell-Douglas MD-80/ 82/
MD83	McDonnell-Douglas MD-80/ 83/
MD87	McDonnell-Douglas MD-80/ 87/
MD88	McDonnell-Douglas MD-80/ 88/
MD90	McDonnell-Douglas MD-90
L101	Lockheed Tristar L101
F100	Fokker100
IL62	Ilyushin IL-62/-62M/MK
N260	Aerospatiale 260 Super Broussard
T154	Tupolev 154/154A/B/B2/C/M

continued on the next page

continued

A/C Code	Aircraft Name
T204	Tupolev 204 204-200 204-220
TU34	Tupolev Tu-34
T34T	T-34C Turbo Mentor
YK40	Yakolev YAK-40
YK42	Yakolev YAK-42

Table A.1: List of aircraft types [16, 27, 28].

Appendix B

Surrogate Model for CO Emissions Estimation

Table B.1 tabulates the description of the engine type codes used in Appendices B, C, and D.

Engine type code	Description
AA	AO 'Aviadgatel'
BR	BMW Rolls-Royce
CM	CFM International
GE	General Electric
IA	International Aero Engines
KK	KKBM
PW	Pratt & Whitney Aircraft Group
RR	Rolls-Royce Ltd
TL	Textron Lycoming
ZM	ZMKB

Table B.1: List of engine type codes.

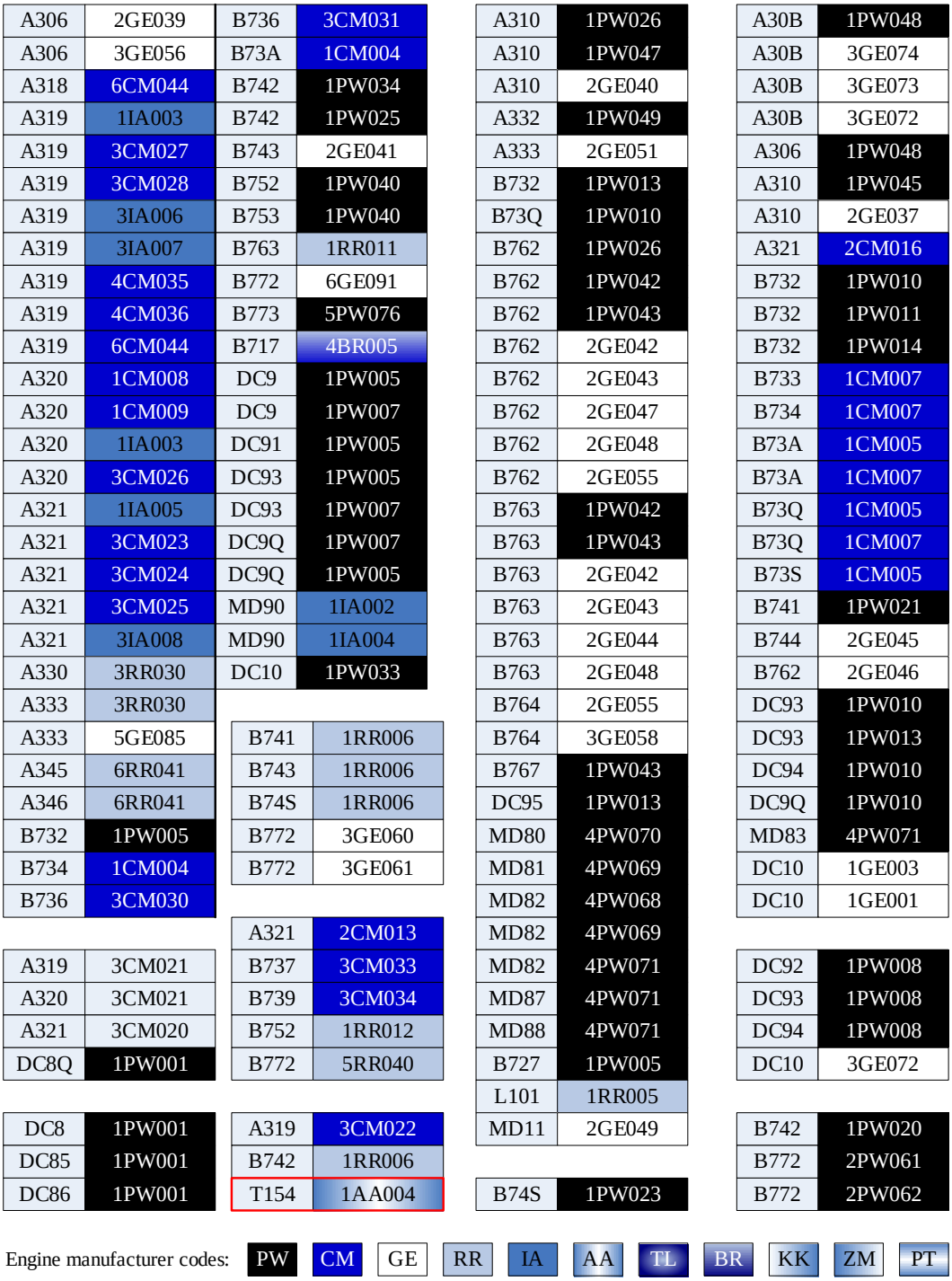

Figure B-1: Part 1: Agents formed for *CO* emissions aggregation, with threshold value 15%, and the total estimation error 0.30%. The formed agents are identified by the spatial clusterings of AE pairs, and the colors differentiate the engine manufacturers.

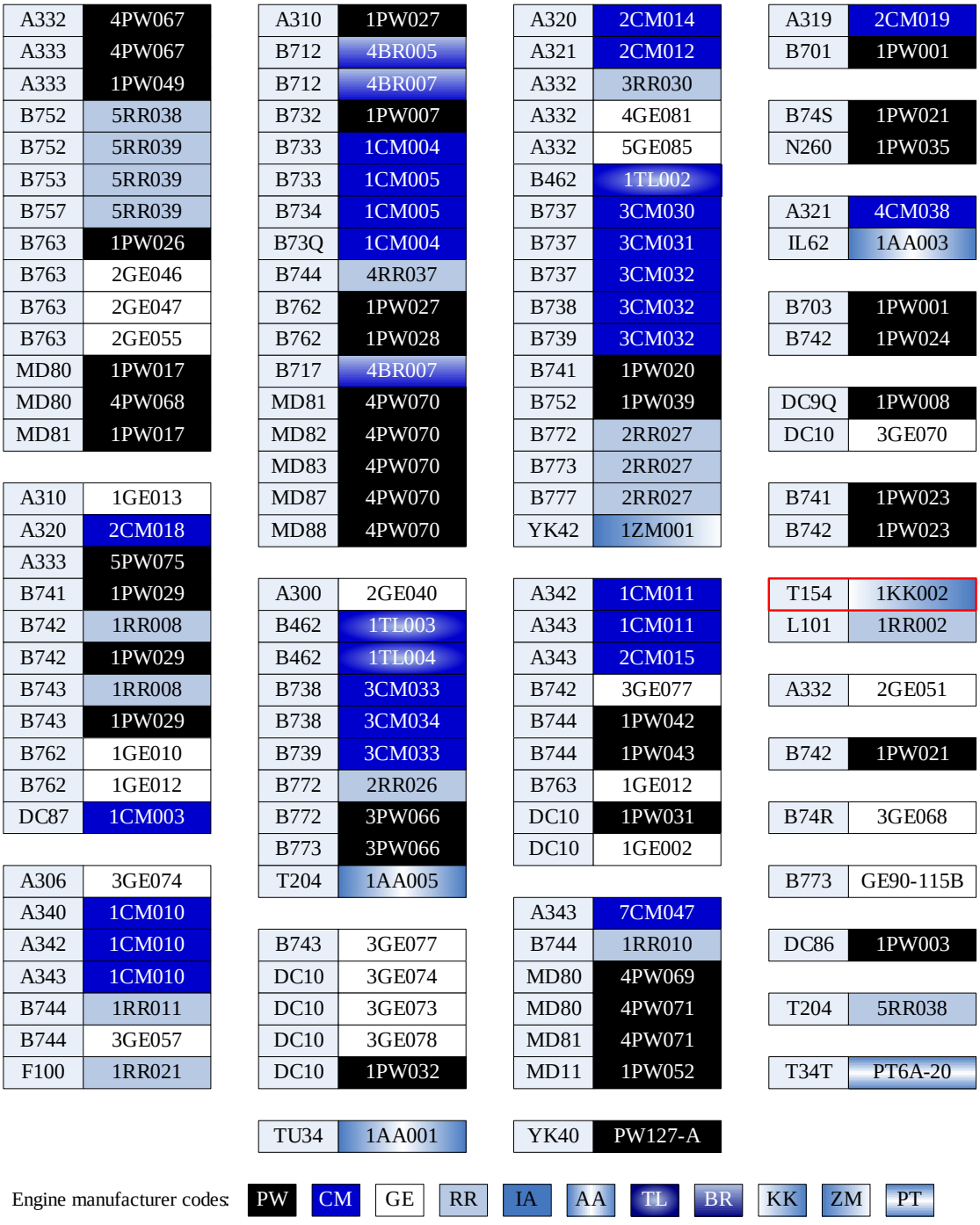

Figure B-2: Part 2: Agents formed for *CO* emissions aggregation, with threshold value 15%, and the total estimation error 0.30%. The formed agents are identified by the spatial clusterings of AE pairs, and the colors differentiate the engine manufacturers.

Appendix C

Surrogate Model for HC Emissions Estimation

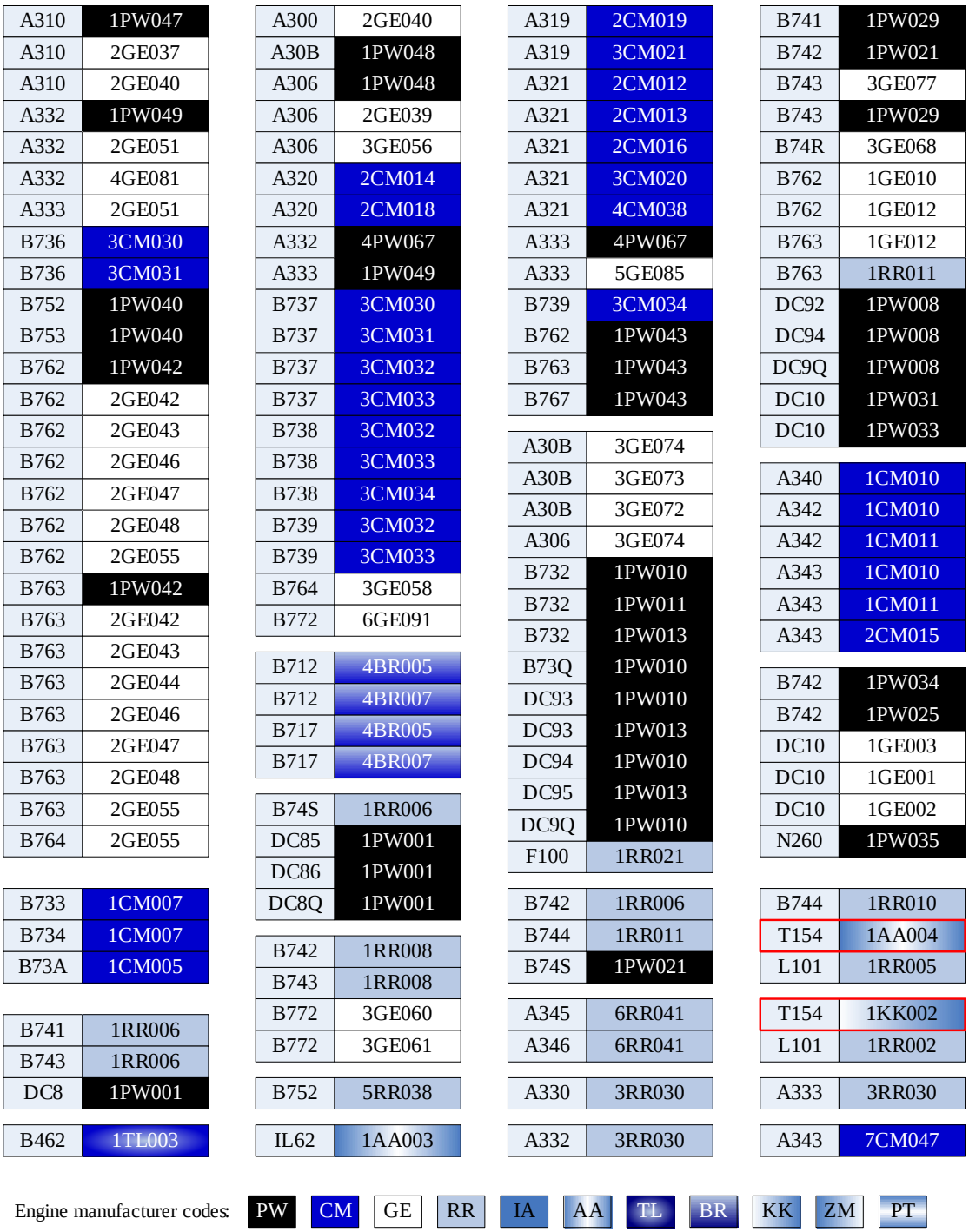

Figure C-1: Part 1: Agents formed for *HC* emissions aggregation, with threshold value 15%, and the total estimation error 0.99%. The formed agents are identified by the spatial clusterings of AE pairs, and the colors differentiate the engine manufacturers.

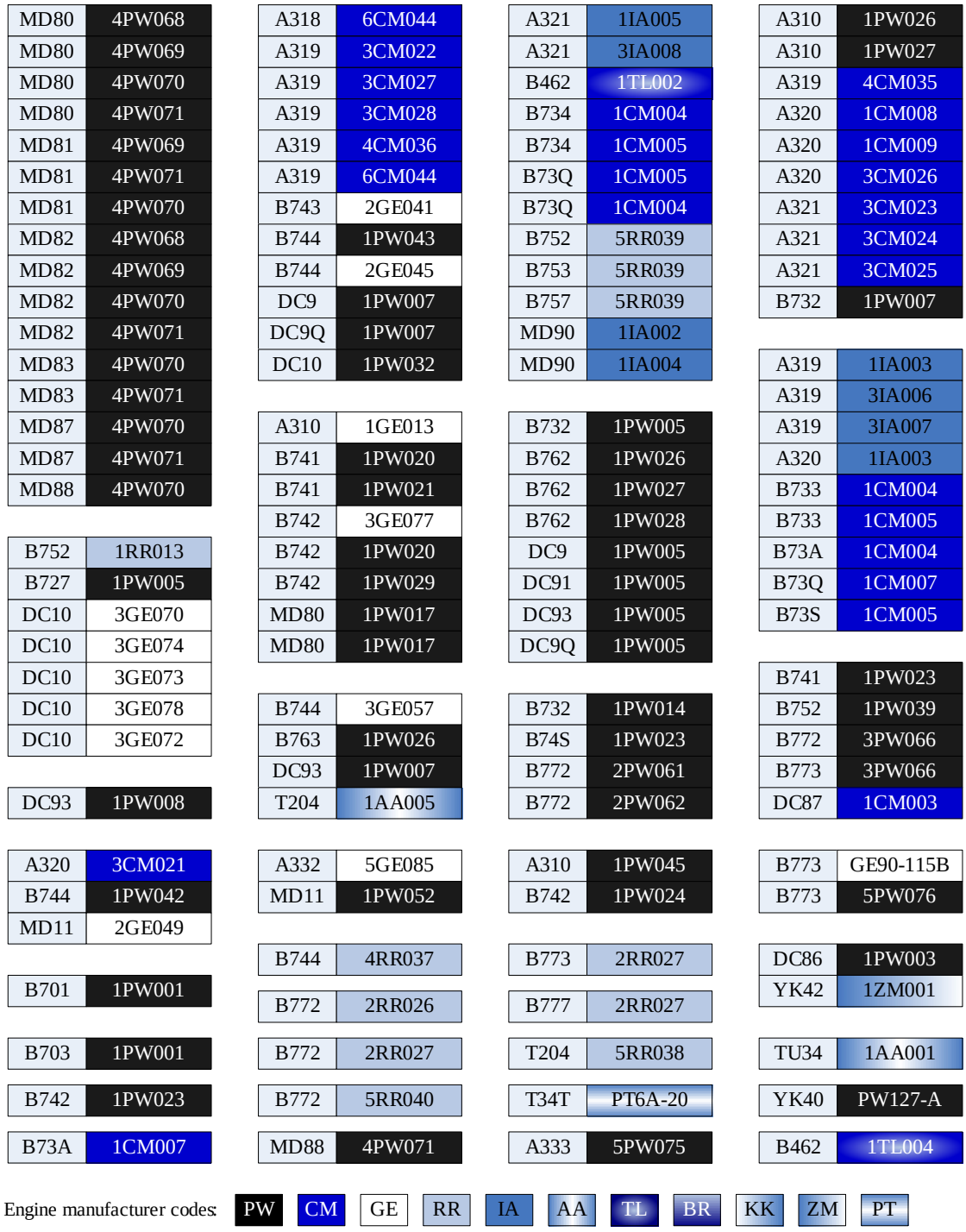

Figure C-2: Part 2: Agents formed for *HC* emissions aggregation, with threshold value 15%, and the total estimation error 0.99%. The formed agents are identified by the spatial clusterings of AE pairs, and the colors differentiate the engine manufacturers.

Appendix D

Surrogate Model for CO_2, H_2O, and SO_x Emissions Estimation

A310	1GE013	B762	2GE043
A310	1PW026	B762	2GE046
A310	1PW027	B762	2GE047
A310	1PW045	B762	2GE048
A310	1PW047	B762	2GE055
A310	2GE037	B763	1GE012
A310	2GE040	B763	1PW042
A330	3RR030	B763	1PW043
A333	5PW075	B763	1RR011
A333	3RR030	B763	2GE042
A333	4PW067	B763	2GE043
A333	2GE051	B763	2GE044
A333	5GE085	B763	2GE046
A333	1PW049	B763	2GE047
B762	1GE010	B763	2GE048
B762	1GE012	B763	2GE055
B762	1PW026	B764	2GE055
B762	1PW027	B764	3GE058
B762	1PW028	B767	1PW043
B762	1PW042	DC87	1CM003
B762	1PW043	DC8Q	1PW001
B762	2GE042		

A320	1CM008	B738	3CM034
A320	1CM009	B739	3CM032
A320	1IA003	B739	3CM033
A320	2CM014	B73A	1CM007
A320	2CM018	B73Q	1CM005
A320	3CM021	B73Q	1PW010
A320	3CM026	B73Q	1CM004
A321	1IA005	B73Q	1CM007
A321	3IA008	DC91	1PW005
B732	1PW007	DC93	1PW005
B732	1PW010	DC93	1PW007
B732	1PW011	DC93	1PW008
B732	1PW013	DC93	1PW010
B732	1PW014	DC94	1PW008
B732	1CM004	DC94	1PW010
B734	1CM004	DC95	1PW013
B734	1CM005	DC9Q	1PW007
B734	1CM007	DC9Q	1PW008
B738	3CM032	DC9Q	1PW010
B738	3CM033	DC9Q	1PW)05

A300	2GE040		
A30B	1PW048	A332	2GE051
A30B	3GE073	A332	3RR030
A30B	3GE072	A332	4GE081
A306	1PW048	A332	4PW067
A306	2GE039	A332	5GE085
A306	3GE056	A345	6RR041
A306	3GE074	B701	1PW001
A332	1PW049	B772	2RR026

		DC10	1PW033
B703	1PW001	DC10	3GE070
B74S	1PW021	DC10	3GE074
B773	GE90-115B	DC10	3GE078
B773	2RR027	DC10	3GE072
B773	5PW076	DC10	1PW032
DC10	1PW031	DC10	1GE002
DC10	1GE003	MD11	1PW052
DC10	1GE001	MD11	2GE049

Engine manufacturer codes: PW CM GE RR IA AA TL BR KK ZM PT

Figure D-1: Part 1: Agents formed for CO_2, H_2O, and SO_x emissions aggregation, with threshold value 15%, and the total estimation error 0.38%. The formed agents are identified by the spatial clusterings of AE pairs, and the colors differentiate the engine manufacturers.

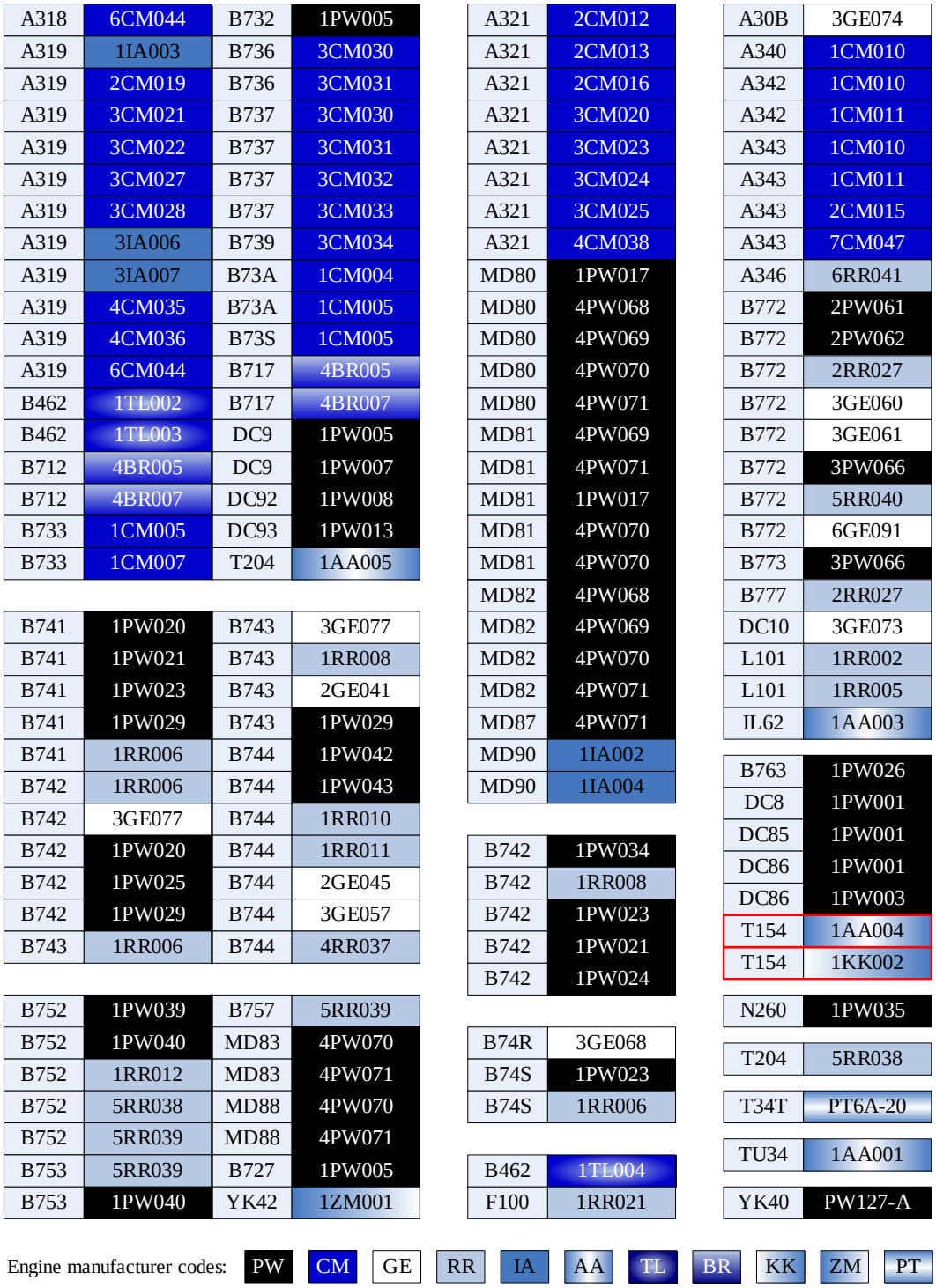

Figure D-2: Part 2: Agents formed for CO_2, H_2O, and SO_x emissions aggregation, with threshold value 15%, and the total estimation error 0.38%. The formed agents are identified by the spatial clusterings of AE pairs, and the colors differentiate the engine manufacturers.

Bibliography

[1] Antoulas, A.C. *Approximation of large-scale dynamical systems*. SIAM, Philadelphia, 2005.

[2] Antoulas, A.C., Sorensen, D.C., Gugercin, S. A survey of model reduction methods for large-scale systems. *Contemporary Mathematics*, 280:193–219, 2001.

[3] Alexandrov, N., Lewis, R.M., Gumbert, C.M., Green, L.L., and Newman, P.A. Approximation and model management in aerodynamic optimization with variable-fidelity models. *Journal of Aircraft*, 38(6):1093–1101, November–December 2001.

[4] Alexandrov, N.M., Lewis, R.M., Gumbert, C.R., Green, L.L., and Newman, P.A. Optimization with variable-fidelity models applied to wing design. *Proceedings of the 38th Aerospace Sciences Meeting and Exhibit*, AIAA Paper 2000-0841, Reno, NV, January 2000.

[5] Alexandrov, N.M., Nielsen, E.J., Lewis, R.M., and Anderson, W.K. First-Order Model Management with Variable Fidelity Physics Applied to Multi-Element Airfoil Optimization. *Proceedings of the 8th AIAA/USAF/NASA/ISSMO Symposium on Multidisciplinary Analysis and Optimization*, AIAA Paper 2000-4886, Long Beach, CA, September 2000.

[6] Barrault, M., Nguyen, N.C., Maday, Y., and Patera, A.T. An "empirical interpolation" method: Application to efficient reduced-basis discretization of partial differential equations. *C.R. Acad. Sci. Paris, Serié I.*, 339:667–672, 2004.

[7] Bertsimas, D., and Tsitsiklis, J.N. *Introduction to Linear Optimization*. Athena Scientific, Belmont, 1997.

[8] Bieniawski, S.R. *Distributed Optimization and Flight Control Using Collectives*. PhD Thesis, Stanford University, October 2005.

[9] Briggs, W.L., Henson, V.E., and McCormick, S.F. *A Multigrid Tutorial*. 2nd ed. SIAM, Philadelphia, 2000.

[10] Choi, S., Alonso, J., Kim, S., and Kroo, I. Two-Level Multifidelity Design Optimization Studies for Supersonic Jets. *43rd AIAA Aerospace Sciences Meeting and Exhibit*, AIAA Paper 2005-531, Reno, NV, January 2005.

[11] Cressie, N. *Statistics of Spatial Data*. John Wiley and Sons, New York, 1991.

[12] Deane, A.E., Kevrekidis, I.G., Karniadakis, G.E., Orszag, S.A. Low-dimensional models for complex geometry flows: Application to grooved channels and circular cylinders. *Phys. Fluids*, 3(10):2337–2354, 1991.

[13] Eldred, M.S., Giunta, A.A., Collis, S.S., Alexandrov, N.A., and Lewis, R.M. Second-Order Corrections for Surrogate-Based Optimization with Model Hierarchies. *Proceedings of the 11th AIAA/ISSMO Multidisciplinary Analysis & Optimization Conference*, AIAA Paper 2004-4457, Albany, NY, August 30–September 1 2004.

[14] Endres, G. *The Illustrated Directory of Modern Commercial Aircraft.* Salamander Books, United Kingdom, 2001.

[15] European Organization for the Safety of Air Navigation. *User Manual for the Base of Aircraft Data (BADA) Revision 3.3.* France, December 2000.

[16] European Organization for the Safety of Air Navigation. *User Manual for the Base of Aircraft Data (BADA) Revision 3.6.* EEC Note No. 10/04, July 2004.

[17] FAA. *SAGE Detailed System Architecture and Design Specification.* Office of Environment and Energy, United States Federal Aviation Administration, Washington, D.C. March 2003.

[18] Feldmann, P., and Freund, R.W. Efficient Linear Circuit Analysis by Padé Approximation via the Lanczos Process. *IEEE Transactions on Computer-Aided Design of Integrated Circuits and Systems*, 14:639–649, 1995.

[19] Ferber, J. *Multi-Agent Systems: An Introduction to Distributed Artificial Intelligence.* Addison-Wesley, England, 1999.

[20] Forrester, A.I.J., Bresslof, N.W., and Keane, A.J. Optimization using surrogate models and partially converged computational fluid dynamics simulations. *Proceedings of the Royal Society A*, 462:2177–2204, March 2000.

[21] Friedman, J. and Stuetzle, W. Projection Pursuit regression. *J. Amer. Statis. Assoc.*, 76:817–823, 1981.

[22] Gallivan, K., Grimme, E., and Van Dooren, P. Padé Approximation of Large-scale Dynamic Systems with Lanczos Method. *Proceedings of the 33rd IEEE Conference on Decision and Control*, December 1994.

[23] Giunta, A.A., Use of data sampling, surrogate models, and numerical optimization in engineering design. *40th AIAA Aerospace Sciences Meeting and Exhibit*, AIAA Paper 2002-0538, Reno, NV, January 14–17 2002.

[24] Grimme, E. *Krylov Projection Methods for Model Reduction.* PhD Thesis, Coordinated-Science Laboratory, University of Illinois at Urbana-Champaign, 1997.

[25] Gugercin, S. and Antoulas, A. A survey of model reduction by balanced truncation and some new results. *International Journal of Control*, 77:748–766, 2004.

[26] Holmes, P., Lumley, J.L., and Berkooz, G. *Turbulence, Coherent Structures, Dynamical Systems and Symmetry.* Cambridge University Press, Cambridge, UK, 1996.

[27] Source of information for aircraft types:
`http://www.airliners.net/info/`

[28] Source of information for aircraft types:
`http://www.aopa.org/whatsnew/acdesig.html`

[29] Eurocontrol's Base of Aircraft Data (BADA):
`http://www.eurocontrol.int/eec/public/standard_page/ACE_bada.html`

[30] International Civil Aviation Committee on Aviation Environmental Protection (ICAO-CAEP). *U.S. Federal Aviation Administration Environmental Tools Suite Assess-*

ment/Evaluation Effort. Modeling and Database Task Force (MODTF) Second Meeting. CAEP/8-MODTF/2-IP/03, Cincinnati, Ohio, July 17–19 2007.

[31] International Civil Aviation Organization Committee on Aviation Environmental Protection (ICAO-CAEP), 2004b. *Report of the FESG/CAEP/6 Traffic and Fleet Forecast (Forecasting Sub-Group of FESG).* CAEP/6-IP/28 Appendix A, Montreal, February 2004.

[32] King, D. and Waitz, I.A. *Assessment of the effects of operational procedures and derated thrust on American Airlines B777 emissions from London's Heathrow and Gatwick airports.* Partnership for Air Transportation Noise and Emissions Reduction (PARTNER), Report No.: PARTNER-COE-2005-001, 2005.

[33] Koehler, J.R. and Owen, A.B. Computer Experiments. In Ghosh, S. and Rao, C.R., editors, *Handbook of Statistics, Volume 13*, Elsevier Science, New York, 1996.

[34] Lee J.J. *Modeling Aviation's Global Emissions, Uncertainty Analysis, and Applications to Policy.* PhD Thesis, Massachusetts Institute of Technology, February 2005.

[35] Lewis, R.M., and Nash, S.G., A Multigrid Approach to the Optimization of Systems Governed by Differential Equations. *Proceedings of the 8th AIAA/USAF/NASA/ISSMO Symposium on Multidisciplinary Optimization*, AIAA Paper 2000-4890, Long Beach, CA, September 2000.

[36] Li, J. and White, J. Low rank solution of Lyapunov equations. *SIAM Journal on Matrix Analysis and Applications*, 24(1):260–280, 2002.

[37] Lukachko, S.P. *The environmental costs of commercial aircraft noise and emissions in the United States.* PhD Thesis, Massachusetts Institute of Technology, 2007 (expected).

[38] Lustick, I.S. Agent-based modelling of collective identity: testing constructivist theory. *Journal of Artificial Societies and Social Simulation*, 3(1), Jan 2000.

[39] Mack, Y., Goel, T., Shyy, W., Haftka, R., and Queipo, N. Multiple Surrogates for the Shape Optimization of Bluff Body-Facilitated Mixing. *43rd AIAA Aerospace Sciences Meeting and Exhibit*, AIAA Paper 2005-333, Reno, NV, January 10–13 2005.

[40] McDonald, D., Grantham, W., Tabor, W., and Murphy, M. Response surface model development for global/local optimization using radial basis functions. *Proceedings of the 8th AIAA/USAF/NASA/ISSMO Symposium on Multidisciplinary Analysis and Optimization*, AIAA Paper 2000-4776, Long Beach, CA, September 2000.

[41] Neter, J., Wasserman, W., and Kutner, M.H. *Applied Linear Statistical Models: regression, analysis of variance, and experimental designs.* Irwin, Homewood, 1990.

[42] Otto, J.C., Landman, D., Patera, A.T. A surrogate approach to the experimental optimization of multielement airfoils. *Proceedings of the 6th AIAA/NASA/ISSMO Symposium on Multidisciplinary Analysis and Optimization*, AIAA Paper 1996-4138, Bellevue, WA, 1996.

[43] Penzl, T. Algorithm for model reduction of large dynamical systems. *Linear Algebra and its Applications*, 415(2–3):322–343, June 2006.

[44] Queipo, N.V., Haftka, R.T., Shyy, W., Goel, T., Vaidyanathan, R., Tucker, P.K. Surrogate-based analysis and optimization. *Progress in Aerospace Sciences*, 41:1–28, 2005.

[45] Robinson, T.D., Eldred, M.S., Willcox, K.E., and Haimes, R. Strategies for Multifidelity Optimization with Variable Dimensional Hierarchical Models. *47th AIAA/ASME/ASCE/AHS/ASC Structures, Structural Dynamics, and Materials Conference*, AIAA Paper 2006-1819, Newport, RI, May 1–4 2006.

[46] Robinson, T.D. *Surrogate-Based Optimization using Multifidelity Models with Variable Parameterization.* PhD Thesis, Massachusetts Institute of Technology, May 2007.

[47] Simpson, T.W., Lin, D.K.J., and Chen, W. Sampling Strategies for Computer Experiments: Design and Analysis. *International Journal of Reliability and Application.*, 2(3):209–240, 2001.

[48] Sirovich, L. Turbulence and the dynamics of coherent structures. Part 1: Coherent structures. *Quarterly of Applied Mathematics*, 45(3):561–571, October 1987.

[49] Sorensen, D.C. and Antoulas, A.C. The Sylvester equation and approximate balanced reduction, *Linear Algebra and its Applications*, 351–352:671–700, 2002.

[50] Steffen, C.J., Jr. Fuel Injector Design Optimization for an Annular Scramjet Geometry. *41st AIAA Aerospace Sciences Meeting and Exhibit*, AIAA Paper 2003-0651, Reno, NV, January 6–9 2003.

[51] Venter, G., Haftka, R.T., and Starnes, J.H., Jr. Construction of Response Surface Approximations for Design Optimization. *AIAA Journal*, 36(12):2242–2249, December 1998.

[52] Waitz, I.A. *et al. Architecture Study for the Aviation Environmental Portfolio Management Tool.* Partnership for Air Transportation Noise and Emissions Reduction (PARTNER), Report No.: PARTNER-COE-2006-002, 2006.

[53] Waitz, I.A. *et al. Requirements Document for the Aviation Environmental Portfolio Management Tool (APMT).* Partnership for Air Transportation Noise and Emissions Reduction (PARTNER), Report No.: PARTNER-COE-2006-001, 2006.